SILICON DENDRITIC WEB MATERIAL PROCESS DEVELOPMENT

9950-684

D. L. Meier, R. B. Campbell, L. J. Stankiewicz, and F. Rai-Choudhury

Final Report

March 1982

Contract 955624

This work was performed for the Jet Propulsion Laboratory, California Institute of Technology under NASA Contract 955624 for the U.S. Department of Energy.

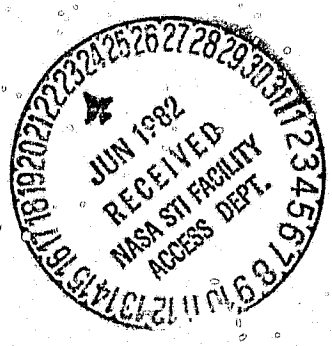

Westinghouse R&D Center
1310 Beulah Road
Pittsburgh, Pennsylvania 15235

SILICON DENDRITIC WEB MATERIAL PROCESS DEVELOPMENT

D. L. Meier, R. B. Campbell, L. J. Sienkiewicz, and
P. Rai-Choudhury

Final Report

March 1982

Contract 955624

This work was performed for the Jet Propulsion Laboratory, California Institute of Technology under NASA Contract 955624 for the U.S. Department of Energy.

Westinghouse R&D Center
1310 Beulah Road
Pittsburgh, Pennsylvania 15235

TABLE OF CONTENTS

Table of Contents (cont'd.)

LIST OF FIGURES

List of Figures (cont'd.)

LIST OF TABLES

1. SUMMARY

The purpose of this program was to develop a low-cost contact system for solar cells and to integrate techniques for fabricating, interconnecting, and encapsulating solar cells in order to produce several demonstration modules. Two experimental contact systems were examined and compared to a baseline contact system consisting of evaporated layers of titanium, palladium, and silver and an electroplated layer of copper. The first experimental contact system consisted of evaporated layers of titanium, nickel, and copper and an electroplated layer of copper. This system performed at least as well as the baseline system in all respects, including its response to temperature stress tests, to a humidity test, and to an accelerated aging test. In addition, the cost of this system is estimated to be only 43% of the cost of the baseline system at a production level of 25 MW/year.

The second experimental contact system consisted of evaporated layers of nickel and copper and an electroplated layer of copper. Auger electron spectroscopy was used to show that the evaporated-nickel layer is not an adequate barrier to copper diffusion at temperatures at least as low as 250°C. This fact brings into question the long-term reliability of this contact system. This system was further afflicted with problems of adherence between the silicon and the evaporated nickel, and for these reasons is not viewed as a promising contact system.

Three modules were fabricated using cells made from dendritic web silicon. Ultrasonic seam bonding was used to interconnect the cells into strings, and ethylene vinyl acetate was used to encapsulate these cell strings. The first two modules were of nominal (30 x 60) cm size and the third module was of nominal (36 x 118) cm size. The efficiency of the third module was measured in natural sunlight to be 10.6%.

2. INTRODUCTION

This program is concerned with two major areas. The first area is the development of a low-cost and reliable contact system for solar cells. The second area is the fabrication of several solar cell modules using ultrasonic bonding for the interconnection of cells and ethylene vinyl acetate as the potting material for module encapsulation. The cells in the modules were made from dendritic web silicon.

Prior to this program, a contact system consisting of thin, evaporated layers of titanium, palladium, and silver, and a thicker electroplated layer of silver was used. In the interest of reducing costs, the electroplated layer of silver was replaced with an electroplated layer of copper. The modules that were fabricated during this program used this evaporated Ti, Pd, Ag and electroplated-Cu (TiPdAg/Cu) system. However, further material cost reductions are possible if the evaporated Pd and Ag layers can be replaced by Ni to give an evaporated Ti, Ni, Cu and electroplated-Cu (TiNiCu/Cu) system. The purpose of Pd is to act as a galvanic buffer to prevent corrosion between Ti and Ag. If Pd is to be eliminated, it must be demonstrated that the TiNiCu/Cu system is not prone to degradation by corrosion. In this study both the TiPdAg/Cu system and the TiNiCu/Cu system are subjected to a humidity test in order to make a comparative check of this mechanism for degradation. In all these cases, Ti is used because it makes an adherent contact to Si and because it acts as a diffusion barrier to the metals above it.

If one wishes to consider a totally plated metal system, then Ti must be eliminated because it cannot be plated on Si. A promising choice, which is being pursued elsewhere,[1] is a Ni Cu system. With proper technique, Ni can be plated on Si. Adherence of Ni to Si is improved if a nickel silicide can be formed by heat treatment. A sufficient thickness of Ni must be present to serve as a diffusion barrier to Cu and the Ni itself must not penetrate the silicon and degrade the cell. In this program, controlled thicknesses of Ni are evaporated on the silicon and Cu is then

deposited on the Ni. Questions related to the effectiveness of Ni as a diffusion barrier to Cu and the ease with which a nickel silicide can be formed are addressed.

The second major area of this program involves the fabrication of three modules using dendritic web silicon and employing ultrasonic bonding as the means for interconnecting cells and ethylene vinyl acetate as the potting material. The first two are of nominal 30 x 60 cm size and the third module is of nominal 36 x 118 cm size.

3. TECHNICAL RESULTS

3.1 Development of a Low-Cost Contact System for Solar Cells

Three different contact systems are studied in this program. The baseline system is evaporated Ti,Pd,Ag and electroplated Cu (TiPdAg/Cu). The first experimental system is evaporated Ti,Ni,Cu and electroplated Cu (TiNiCu/Cu). The second experimental system is evaporated or sputtered Ni, evaporated or plated Cu (strike layer), and plated Cu (NiCu/Cu or Ni/Cu/Cu). The response of these systems to heat treatment, thermal stress, and humidity stress is investigated. In addition, the deposition of a thin layer of electroplated Ni on the Cu in the TiPdAg/Cu and the TiNiCu/Cu systems in order to facilitate ultrasonic bonding is examined.

3.1.1 Theoretical Considerations

When a metal is deposited on a semiconductor, the composite system comes to equilibrium by means of a momentary flow of charge from one material to the other. This charge flow equalizes the Fermi level throughout the system and gives rise to a Schottky barrier at the metal/semiconductor interface. The qualitative features of such a Schottky barrier are illustrated in Figure 1 by the band diagram of a metal on an n-type semiconductor.

The characteristics of the barrier are determined by the relative strengths with which electrons are bound to the metal and to the semiconductor as well as by the doping density of the semiconductor. The barrier height, ϕ_B, is given by[2]:

$$\phi_B = \phi_m - \chi_s \qquad (1)$$

where ϕ_m is the work function of the metal (energy required to free an electron at the Fermi level from the metal) and χ_s is the electron affinity of the semiconductor (energy required to free an electron at the bottom of the conduction band from the semiconductor). The built-in or diffusion potential, V_d, of Fig. 1 is given by:

$$eV_d = \phi_m - \phi_s \qquad (2)$$

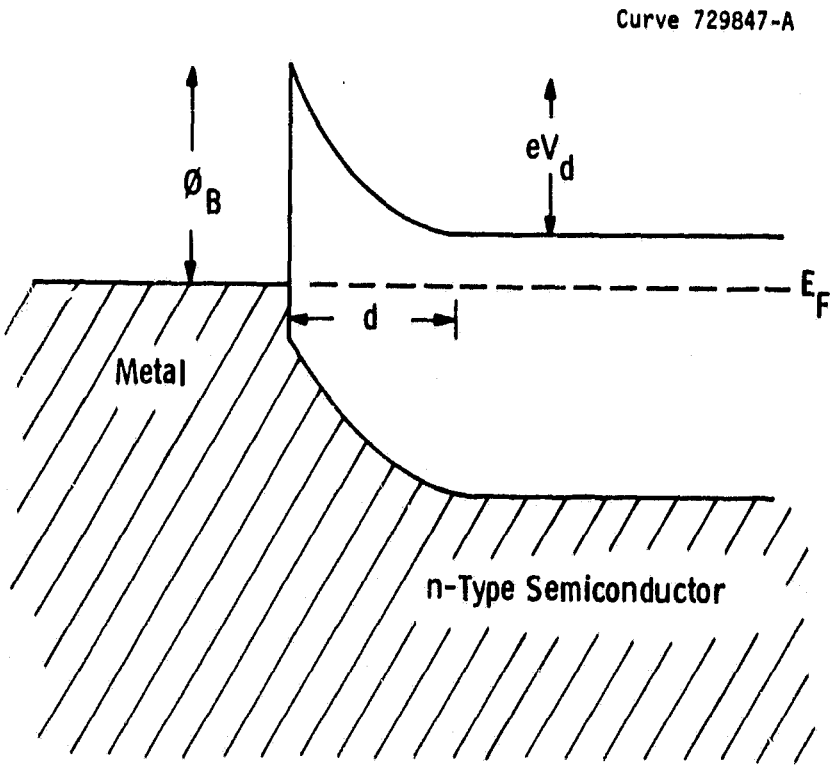

Figure 1. Schottky barrier formed at metal/semiconductor interface.

where e is the magnitude of the electronic charge and ϕ_s is the work function of the semiconductor.

In Figure 1, electrons have been transferred from the semiconductor to the metal upon contact, leaving a layer of width d in the semiconductor which is depleted of free electrons. The width of this depletion region is given by:

$$d = \sqrt{(2\varepsilon\varepsilon_0/eN_d)(V_d+V)} \qquad (3)$$

where ε_0 is the permittivity of free space, ε is the relative dielectric constant for the semiconductor, N_d is the doping concentration for the semiconductor, and V is the externally applied voltage, measured relative to the metal. The energy of the conduction band edge, E_C, relative to the Fermi energy, E_F, varies parabolically within the depletion region and is given by[3]:

$$E_C - E_F = \phi_B = (e^2N_d/2\varepsilon\varepsilon_0)(xd = x^2/2) \qquad (4)$$

for $0 \leq x \leq d$.

There are essentially two ways by which electrons can be transferred from the semiconductor to the metal. These are thermionic emission, in which electrons have sufficient thermal energy to pass over the top of the barrier, and field emission, in which electrons tunnel through the barrier.[4] These mechanisms are analogous to those which occur in a metal. If the metal is heated to a sufficiently high temperature so that electrons can be "boiled" off the surface, then these electrons are said to escape by thermionic emission. If the metal is immersed in a strong electric field ($\sim 10^9$ V/m) that changes the potential energy well in which the electrons move within the metal, then the electron can escape by quantum mechanical tunneling through the thin walls of the potential well. These electrons are said to escape by field emission.

Whether the dominant current transport mechanism at room temperature is "thermionic emission" over the barrier or "field emission" through the barrier depends on the doping density of the semiconductor. If the doping density is less than $10^{18}/cm^3$, then the dominant mechanism is "thermionic emission" and, if it is greater than $10^{18}/cm^3$, the dominant

mechanism is "field emission".[5] The effect of the doping density (N_d) can be seen from Equation 3. As N_d increases the depletion width (d) decreases and, with this narrower barrier, electron tunneling becomes more prevalent.

For the contact systems that have been studied in this work, the interface is between either titanium or nickel metal and silicon which has undergone an n^+ diffusion. It is instructive to estimate the Schottky barrier parameters for our systems. The barrier height (ϕ_B) for titanium on n-type silicon is approximately 0.50 eV and for nickel on n-type silicon is approximately 0.68eV.[6] A typical dopant concentration profile for silicon web which has undergone the standard phosphorous diffusion at 850°C is shown in Figure 2. From Figure 2 the surface concentration is seen to be $8.1 \times 10^{19}/cm^3$. Because the semiconductor is heavily doped, the Fermi level lies close to the conduction band edge so $eV_d \sim \phi_B$. The barrier width (d) can now be estimated from Eq. 3 with $\varepsilon_{Si} = 12$, $\varepsilon_o = 55.4$ e/(Vμm), $V_d = 0.5$ V, and $N_d = 8.1 \times 10^{19}/cm^3$. The resultant barrier width is $d \sim 29$Å. Thus, in our case, electrons in the semiconductor have an average thermal energy of ∿0.026 eV above the Fermi level and are faced with an energy barrier ∿ 0.5 eV high and ∿ 29Å thick. These electrons are able to pass from the semiconductor to the metal (and vice-versa) by tunneling through the narrow barrier. It is apparent that as doping density increases, the barrier thickness decreases and the contact becomes more like a metal-to-metal, or ohmic, contact.

The previous description ignored the surface states which may be present at the semiconductor surface prior to joining the semiconductor with the metal.[7] These states are filled with electrons to the Fermi level and so cause the bands to bend and form a barrier on their own accord. This tends to reduce the influence of the metal in determining the height of the Schottky barrier but leaves the previous description of electron transport qualitatively unchanged.

Solar cells fabricated for this contract have an n^+pp^+ structure. Contacts to the front (sunside) of the cell are metal to n^+ silicon, while contacts to the back are metal to p^+ silicon. Behavior of the metal to p^+ silicon is completely analogous to the behavior of the metal to n^+ silicon contact. A band diagram for the complete solar cell with contacts is shown in Figure 3.

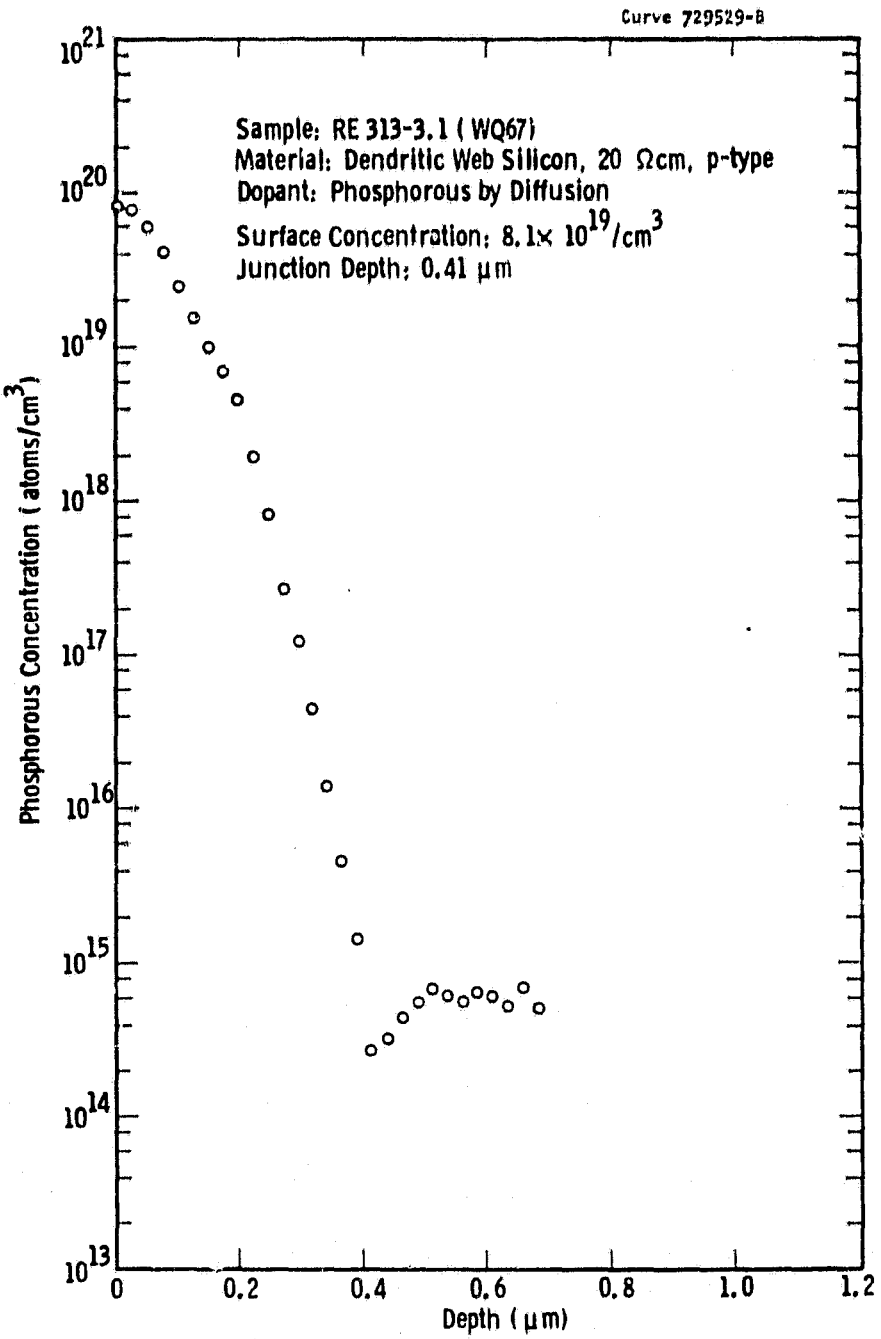

Figure 2. Typical dopant concentration profile for phosphorous-diffused dendritic web silicon.

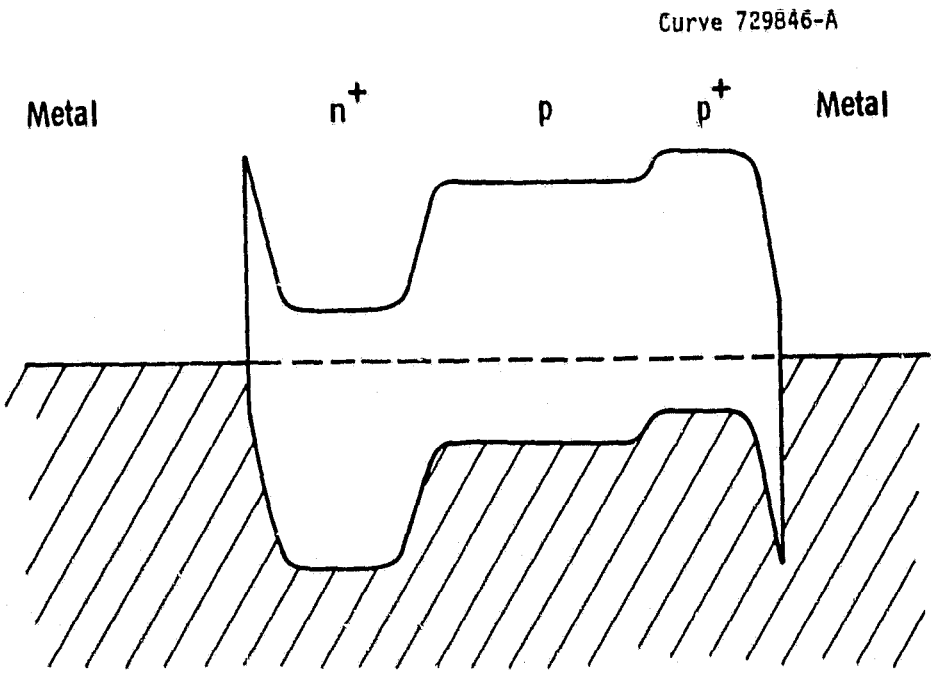

Figure 3. Band diagram for a solar cell, including contacts.

3.1.2 Solar Cell Contact Mask

In Figure 4 is shown the set of two masks that were developed for this work. These masks are suitable for use with 2-inch wafers. The set consists of one mask with several test patterns and a second mask which provides a mesa for the various patterns. In this way several different types of information related to the contacts can be obtained on a homogeneous wafer, all parts of which have undergone identical processing.

The main pattern is a (1.60 x 4.00) cm solar cell located near the center of the wafer. Measurements of points on the lighted I-V curve are used to determine cell efficiency (η), fill factor (FF), short-circuit current density (J_{sc}), and open-circuit voltage (V_{oc}). This is done by fitting the data points (J, V) to an expression of the form:

$$J(V) = J_{sc} - J_o \left(e^{q(V+JR_s/NkT} - 1\right) \qquad (5)$$

in order to extract the parameters J_o (diode reverse-saturation current density), R_s (cell series resistance), and N (diode ideality factor).

In addition, forward diode characteristics are measured for the cell in the dark. These measurements are used primarily to obtain information regarding the quality of the junction region. Estimates of the shunt and series resistance of the cell are also obtained from measurements in the dark. Shunt resistance (R_{sh}) is estimated by measuring the leakage current (J_R) at a reverse bias of -1 V:

$$R_{sh} = -1V/J_R \qquad (6)$$

Series resistance is given by the relation [8]:

$$R_s = [V_F(J = J_{sc}) - V_{oc}]/J_{sc} \qquad (7)$$

where V_F is the forward dark voltage required to obtain a forward dark-current density equal in magnitude to the lighted short-circuit current density (J_{sc}).

Above the cell pattern is a (1.27 x 1.27) cm square which serves two purposes. The first purpose is to act as a large-area diode with which the minority carrier lifetime in the base can be measured by the open-

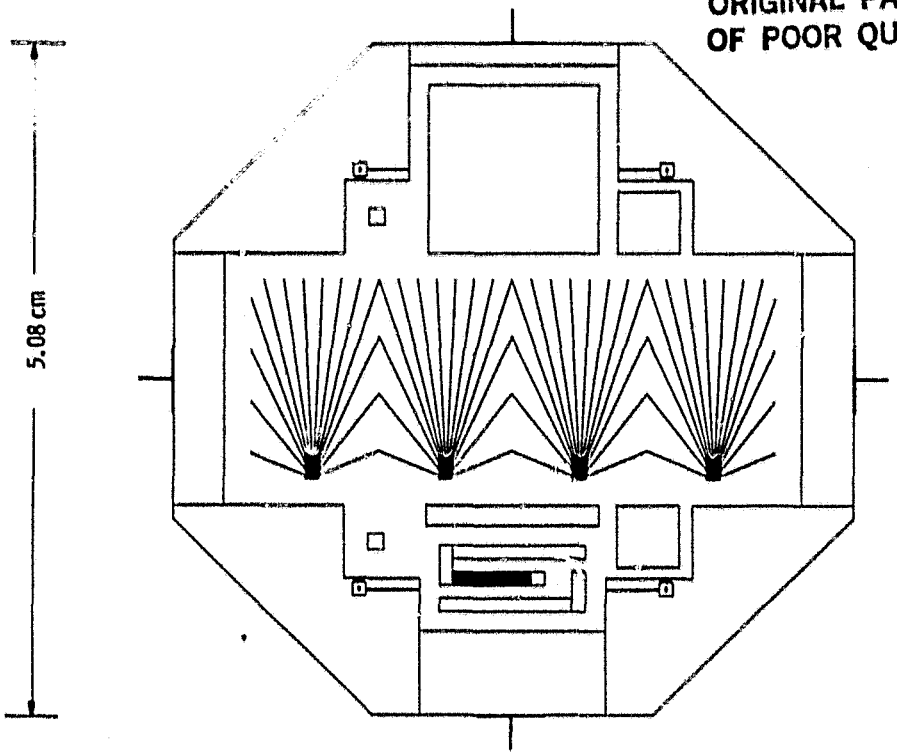

A. Solar cell contact test patterns; cell (1.60 × 4.00 cm), contact resistance (0,50 × 1.09 cm), sheet resistance/OCD-lifetime square (1.27 × 1.27 cm), and smaller area diodes.

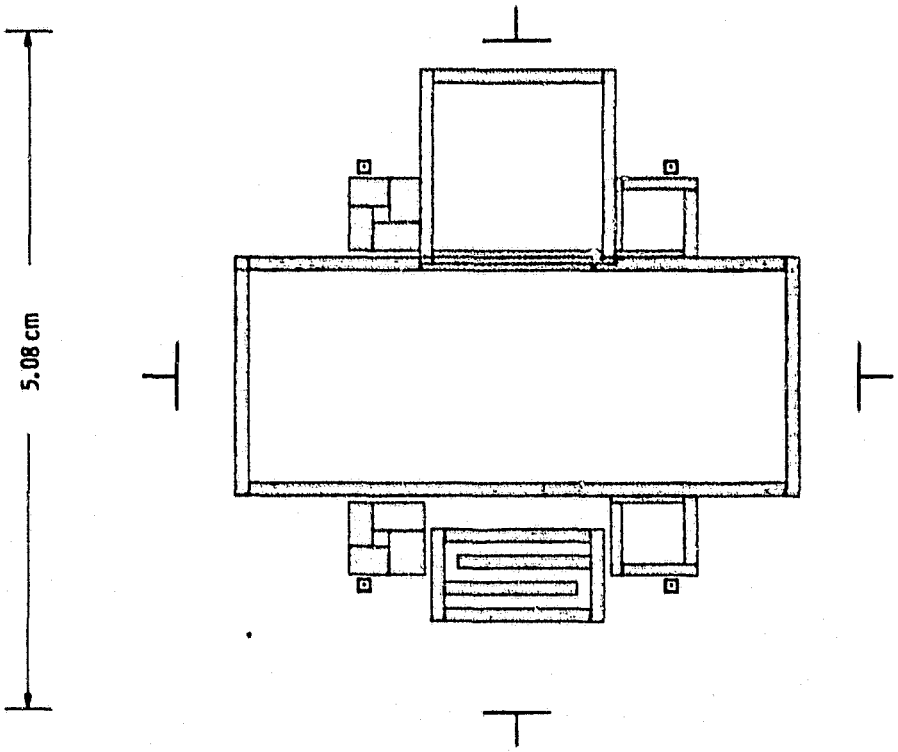

B. Mesa pattern for test patterns of Part A

Figure 4. Solar cell contact masks: test patterns and mesa patterns.

circuit voltage decay method (τ_{ocd}). The second purpose is to act as a well-defined area over which the sheet resistance of the evaporated metal (especially evaporated Ni) can be measured both in the as-deposited state and after heat treatment. By knowing the thickness of the evaporated Ni film, its resistivity can be determined from this measurement of sheet resistance. In addition, this pattern can be used to estimate the thickness of nickel silicide that is formed by heat treatment, provided the resistivity of the silicide is known or can be measured. Since the measurement of sheet resistance involves the use of a four-point probe on a finite area, the relation between sheet resistance ($R_{\square}$) and the measured current (I) and voltage (V) must be specified for the particular dimension of the test square and the probe spacing used.[9] In our case, with probe spacing of 0.127 cm, this relation is:

$$R_{\square} = 4.22\ V/I \qquad (8)$$

Note that the coefficient in Equation 8 is 4.22 rather than 4.53 for the more common case of sheet dimensions very much larger than probe spacing.

Also seen in Figure 4A are two intermediate-sized squares and two small-sized squares. These are simply auxiliary diodes which can be used in special circumstances. The intermediate-sized diodes are available for carrier lifetime (τ_{ocd}) measurements, while the small-sized diodes can be used for deep-level transient spectroscopy (DLTS) measurements.

In the lower part of Figure 4A is a pattern for measuring the contact resistance associated with the interface between the n^+ silicon and the bottom layer of metal in the contact systems. This pattern and its associated mesa are shown in greater detail in Figure 5. There it is seen that the pattern consists of contact pads A, B, and C with a gap between contacts B and C and a series of 39 metal bars between contacts A and B. A mesa pattern, shown in Figure 5B, is used to isolate the available current paths from the remainder of the silicon substrate. The metal bars between A and B are 100 μm wide and are separated by 50 μm. Contact pads B and C are separated by 2000 μm of n^+ silicon. Contact pads A and C are L-shaped in order to accommodate the limited travel of the probes that were used in this work to measure voltage drops V_{AB} and V_{BC}.

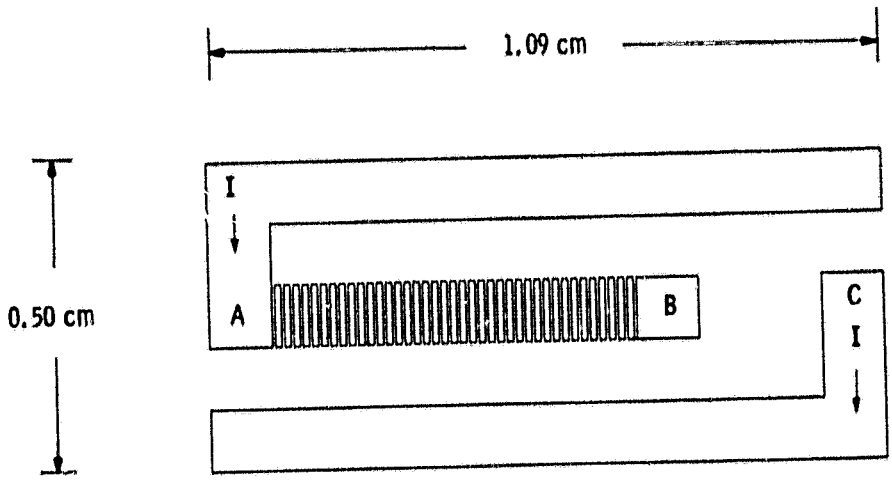

A. Contact resistance test pattern: 39 metal bars of length 1 mm and width 100μm width of gap between bars is 50 μm, and width of large gap between contact pads B and C is 2000 μm

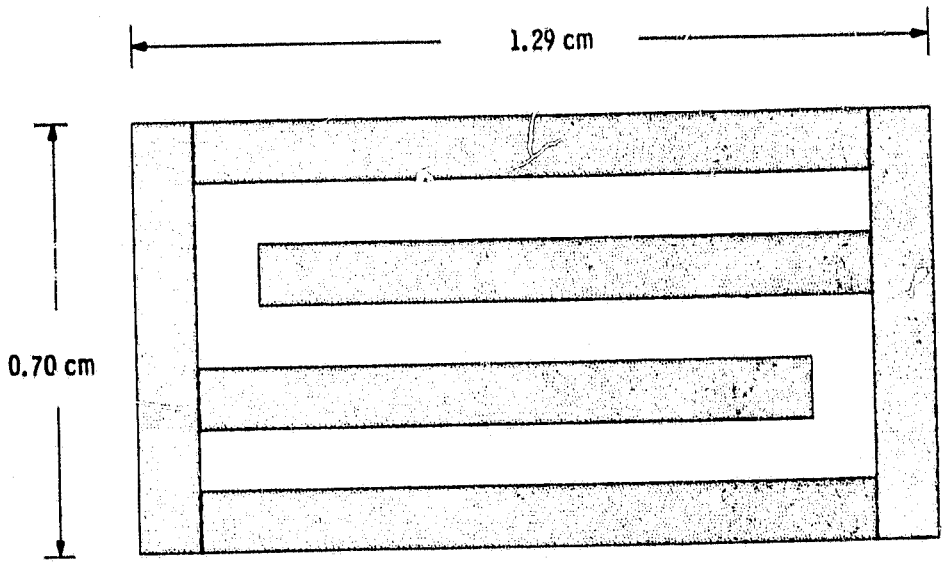

B. Mesa pattern for contact resistance test pattern of Part A

Figure 5. Contact resistance test pattern and mesa pattern.

In using the contact resistance pattern, a current (I) of typically 10 mA is sent from contact A through the strip covered with metal bars to contact B, then through the n^+ region to constant C. The mesa restricts the current flow to one dimension for simplicity in analysis. In passing from A to B, the current travels through the n^+ region between metal bars but transfers to the metal bars over that part of the path which is covered by them. However, the transfer does not occur entirely at the bar edge. Because of the contact resistance between the n^+ substrate and the metal bar, the amount of current remaining in the n^+ substrate falls off exponentially with distance from the edge of the bar.[10] The characteristic length of this exponential current transfer is called the transfer length (L_T).

The voltage drop associated with current flow beneath the contact bar is just equal to the voltage drop that would occur if the current were to flow instead through a length L_T of the n^+ region. When the current flows from the metal bar back into the silicon substrate, it does so exponentially with characteristic length L_T. Consequently, the voltage drop associated with this flow from bar to substrate is again equivalent to the voltage drop that would occur if the current were to flow instead through a length L_T of the n^+ region. It is assumed here that the sheet resistance of the metal bar is negligible compared to the sheet resistance of the n^+ region, so only a negligible voltage drop is associated with current flow through the bar. It can be seen, then, that the voltage drop from A to B is given by:

$$V_{AB} = (IR_{\square})[(n + 1)\ (L_1 + 2\ L_T)/W] \qquad (9)$$

where $R_{\square}$ is the sheet resistance of the n^+ layer, n is the number of metal bars, L_1 is the spacing between bars, and W is the width of the metal bars. Similarly, the voltage drop from B to C is given by:

$$V_{BC} = (I\ R_{\square})[(L_2 + 2\ L_T)/W] \qquad (10)$$

where L_2 is the spacing between pads B and C. From equations 9 and 10 we have

$$V_{AB} - V_{BC} = (IR_{\square})[(n + 1)\ L_1 - L_2 + 2nL_T]/W \qquad (11)$$

Since typically $L_T \lesssim 10$ μm, it can be ignored compared to L_2 which is 2000 μm, and $R_{\square}$ can be obtained from Equation 10 as:

$$R_{\square} \simeq (V_{BC}/I)(W/L_2). \qquad (12)$$

Substituting for $R_{\square}$ in Equation 11 and solving for L_T yields:

$$L_T = [L_2 V_{AB}/V_{BC} - (n + 1)L_1]/2n \qquad (13)$$

Finally, the contact resistance (R_c) is related to the current transfer length (L_T) and the sheet resistance of the diffused n^+ region ($R_{\square}$) by:

$$R_c = R_{\square} L_T^2 \qquad (14)$$

In this work, typical values are $R_{\square} \approx 60\ \Omega/\square$, $L_T \approx 3\ \mu m$, and $R_c \approx 5 \times 10^{-6}\ \Omega cm^2$.

Because the effects of contact resistance are accumulated over the 39 metal bars in this pattern, the measurement is rather precise. It is also convenient to use in that only two voltages (V_{AB} and V_{BC}) and one current (I) need to be measured. However, the accuracy of the measurement does depend on having accurate values of spacing between metal bars (L_1) and spacing between contact pads B and C (L_2), as is evident from Equation 13. Consequently, these dimensions should be measured with an accuracy of better than $\pm$ 1 μm in order to obtain reliable values of transfer length (L_T) for contacts with low resistance.

3.1.3 Process Sequence

The intention in carrying out this work on contacts was to adhere as closely as possible to the sequence that had been developed for processing dendritic web silicon into solar cells. A set of process specifications is given in Appendix A, and the major steps of the sequence are given below:

1. Begin with boron-doped 4 Ω cm, <111> float zone silicon (Monsanto), 250 μm thick or boron-doped 2-11 Ω cm, <111> Dendritic Web silicon, 130-275 μm thick.
2. Form the back junction (p^+p) by a BBr_3 diffusion at 950°C for 37 minutes.
3. Form the front junction (n^+p) by a $POCl_3$ diffusion at 850°C for 30 minutes.

4. Apply an antireflection coating which has an index of refraction of 2.0 and a thickness of 750Å.

5. Apply a positive photoresist and define the patterns of Figure 4A in the photoresist by photolithography.

6. Define the patterns of Figure 4A in the antireflection coating by etching down to bare silicon.

7. Evaporate one of the candidate contact systems (500 Å Ti, 300 Å Pd, 300 Å Ag; 500 Å Ti, 400 Å Ni, 300 Å Cu; 600 Å or 1200 Å Ni, 300 Å Cu; 600 Å or 1200 Å Ni) over the entire front and back surfaces.

8. Form the metal pattern by removing the excess evaporated metal using a lift-off process.

9. Electroplate copper to a thickness of approximately 5 μm on the front and back.

10. Apply a negative photoresist and delineate the various patterns by means of the mesa of Figure 4B.

11. Test.

12. Subject the sample to appropriate heat treatment or stress.

13. Retest.

3.1.4 Sintering Studies for Baseline and First Experimental Contact System

Sintering at modest temperatures (300°C - 500°C) is often used to improve adherence of the contact system and to reduce series resistance in a solar cell. Sintering can also be used as an accelerated aging test in which the effectiveness of a metal layer in acting as a diffusion barrier can be examined.

In this phase of work, samples of both the baseline contact system (evaporated layers of 500 Å Ti, 300 Å Pd, 300 Å Ag and an electroplated layer of 5 μm Cu) and the first experimental contact system (evaporated layers of 500 Å Ti, 400 Å Ni, 300 Å Cu and an electroplated layer of 5 μm Cu) were sintered at temperatures ranging from 300°C to 400°C. An

atmosphere of H_2 flowing through a 109-mm ID tube at 10 ℓ/min was used during sintering. The results are summarized in Tables I and II. In these Tables all data are normalized to an area of 1 cm^2. J_o is the diode reverse-saturation current density of Equation 5 in units of A/cm^2. R_s, R_{sh}, and R_c are the normalized series, shunt, and contact resistances, as described by Equation 7, 6, and 14, respectively.

Generally speaking, both contact systems are able to withstand sintering temperatures up to 400°C, although cell efficiency is observed to degrade somewhat with increased sintering temperature. Only in the cases of NB19 and NB42, where the presintered cell had an inferior fill factor, did the sintering improve cell efficiency. In all other cases, sintering caused a degradation in cell efficiency, especially at 350°C and above. This degradation is reflected most prominently in the parameters Log (J_o) and N, which are indicators of junction quality. An excellent cell ($\eta \sim 15\%$) is usually found to have a value of Log (J_o) near -10 and a value of N near 1.0. As can be seen from Tables I and II, sintering tends to cause both parameters to increase. This is reflected in a decrease in fill factor and consequently in efficiency.

Dark I-V data were taken for each sintering temperature in several cases. The data can be approximated by a relation of the form[11]:

$$J(V) = J_{O1}e^{V/V_T} + J_{02}e^{V/nV_T}, \qquad (15)$$

where $V_T = kT/q$. The first term on the right side of Equation 15 arises from current flow by carrier diffusion through the bulk. The second term on the right describes current flow by recombination in the junction depletion region. A plot of the dark I-V characteristics for sample NB122, which has the baseline contact system, is given in Figure 6. From Table I, one can see that the cell efficiency has gone from 15.1% to 14.5% then to 13.4% with successive sintering steps. The dark I-V plots of Figure 6 show that this degradation is not due to a change in the bulk, since the upper segment of the curve is affected very little. The lower segment is dramatically affected, however, indicating a significant increase in junction recombination current or shunting. These data do not pinpoint the source of the degradation, but it is presumably due to a diffusion of Cu and/or Ag through or along the edges of the Ti layer and into the Si. It might be noted that the parameters Log (J_o)

TABLE I. Effect of Sintering Temperature on Cells

Having the Baseline Contact System

Material: Float Zone Silicon, Boron-doped 4Ωcm, <111>, 250 μm thick
Evaporated: 500Å Ti, 300 Å Pd, 300 Å Ag
Electroplated: 5 μm Cu
Cell Size: (1.60 x 4.00) cm_2
Test Conditions: 91.6 mW/cm^2, AM1, Room Temperature
Heat Treatment: Temperature as noted, 15 min. H_2 at 10 ℓ/min

Sample	Temperature (°C)	J_{sc} (mA/cm^2)	V_{oc} (V)	FF	n(%)	Log (J_o)	N	R_s (Ωcm^2)	R_{sh} ($k\Omega cm^2$)	R_c ($\mu\Omega cm^2$)
NB19	pre-sinter	29.8	0.574	0.657	12.3	-4.3	3.40	1.24	640.	-
	300	28.8	0.586	0.740	13.6	-7.4	1.68	0.94	42.	-
	350	28.4	0.569	0.651	11.5	-4.3	3.47	0.92	15.	-
	400	28.7	0.581	0.660	12.0	-4.7	3.04	1.11	2.0	-
NB72	pre-sinter	30.4	0.585	0.782	15.2	-10.0	1.15	0.72	5.9	-
	300	29.9	0.590	0.782	15.1	-8.9	1.34	0.60	5.6	1.2
	350	24.5	0.572	0.776	13.3	-8.8	1.30	0.99	5.7	-
	400	30.0	0.583	0.765	14.6	-8.6	1.39	0.93	4.7	-
NB114	pre-sinter	29.8	0.547	0.789	14.0	-10.6	1.01	0.44	2.4	3.1
	350	29.6	0.540	0.770	13.4	- 8.6	1.27	0.95	2.6	2.2
	400	29.6	0.538	0.731	12.7	- 6.5	1.80	1.32	.2.6	4.2
NB122	pre-sinter	30.4	0.575	0.793	15.1	-10.3	1.10	0.49	18.	3.0
	350	30.2	0.567	0.776	14.5	- 8.9	1.28	0.79	19.	3.8
	400	30.4	0.565	0.718	13.4	- 5.9	2.14	0.92	14.	9.7

TABLE II. Effect of Sintering Temperature on Cells
Having the First Experimental Contact System

Material: Float Zone Silicon, Boron-doped 4Ωcm, <111> 250 μm thick
Evaporated: 500 Å Ti, 400 Å Ni, 300 Å Cu
Electroplated: 5 μm Cu
Cell Size: (1.60 x 4.00) cm_2
Test Conditions: 91.6 mW/cm^2, AM1, Room Temperature
Heat Treatment: Temperature as noted, 15 min, H_2 at 10 ℓ/min

Sample	Temperature (°C)	J_{sc} (mA/cm^2)	V_{oc} (V)	FF	n(%)	Log (J_o)	N	R_s (Ωcm^2)	R_{sh} ($k\Omega cm^2$)	R_c ($\mu\Omega cm^2$)
NB42	pre-sinter	30.7	0.567	0.717	13.6	-6.6	1.87	1.01	920.	2.2
	300	30.3	0.582	0.741	14.3	-7.4	1.64	0.92	640.	1.6
	350	29.9	0.569	0.736	13.7	-7.4	1.60	1.27	84.	4.9
	400	30.5	0.588	0.698	13.7	-5.9	2.25	1.34	46.	7.3
NB52	pre-sinter	30.5	0.575	0.770	14.8	-9.5	1.20	0.85	6400.	2.4
	300	29.8	0.579	0.784	14.8	-9.9	1.15	0.63	32.	1.8
	350	29.9	0.562	0.752	13.8	-7.5	1.57	1.20	2.5	6.9
	400	29.8	0.578	0.727	13.7	-7.2	1.69	1.71	35.	9.8
NB101	pre-sinter	26.3	0.506	0.782	11.4	-9.9	1.02	0.45	3.6	1.9
	350	25.9	0.499	0.782	11.0	-9.7	1.03	0.54	4.1	1.0
	400	26.4	0.495	0.760	10.8	-8.5	1.19	0.91	4.4	1.8
NB107	pre-sinter	30.7	0.567	0.780	14.8	-9.7	1.15	0.45	0.68	3.1
	350	30.3	0.561	0.776	14.4	-9.5	1.17	0.86	0.73	4.2
	400	30.4	0.563	0.763	14.2	-9.0	1.25	0.95	0.92	5.0

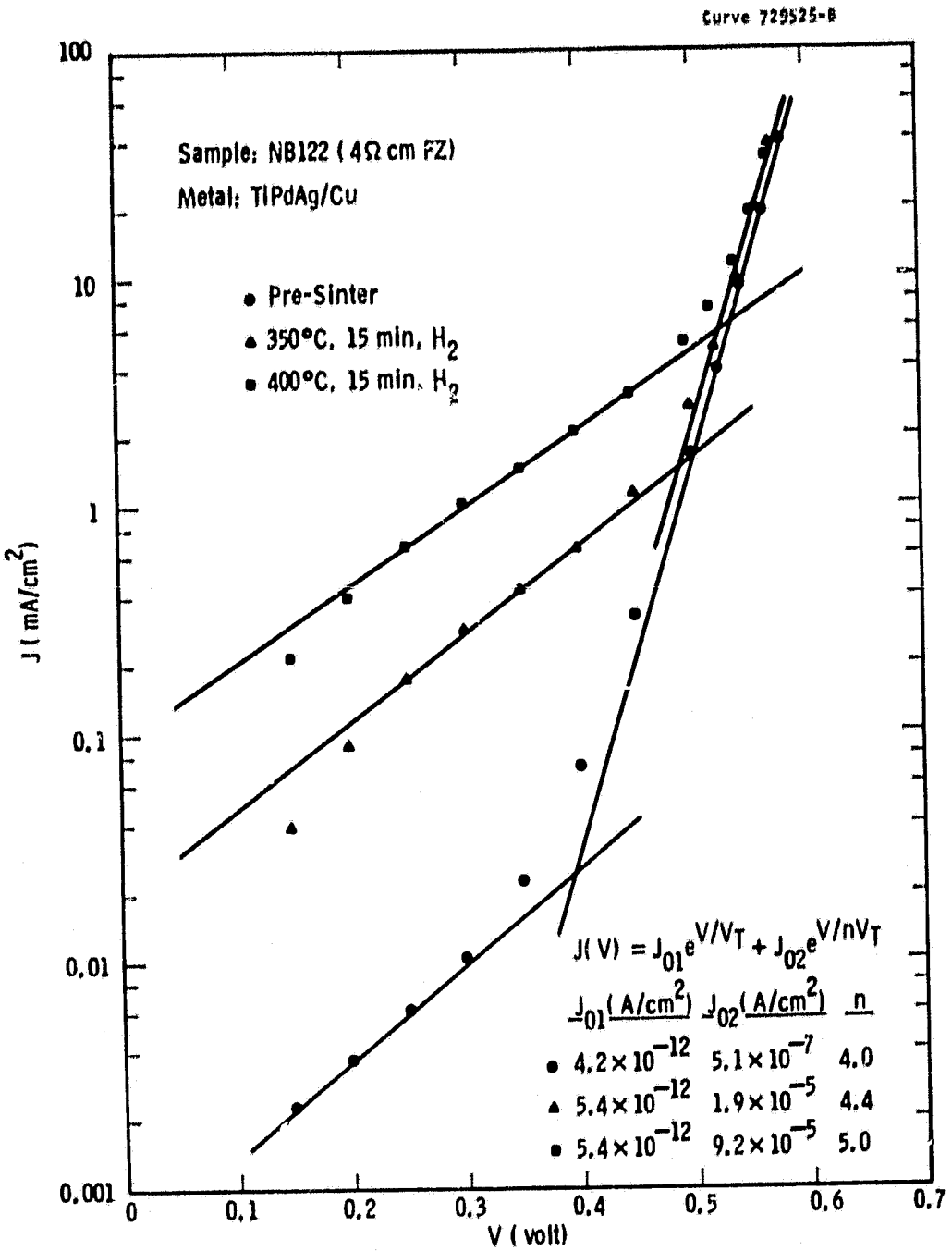

Figure 6. Effect of sintering on dark I-V characteristics for the Ti Pd Ag/Cu system.

and N of Table I for NB122 trace the lower segments of the dark I-V curves, as expected.

Similar curves for samples NB42 and NB107, which have the first experimental contact system, are given in Figures 7 and 8. Again the data of Table II for these samples, particularly η, Log (J_o), and N, track well with the movement of the lower segment of the dark I-V curves. Although it can generally be said that sintering increases the junction recombination current or shunting, the variation in slope and movement of the lower segment of the dark I-V curves in Figures 6,7, and 8 are certainly not fully understood.

From Tables I and II it is seen that both contact systems have excellent contact resistance, with a typical value being 3×10^{-6} Ωcm^2. The normalized series resistance is approximately 0.5 Ωcm^2 for the presintered samples. The normalized shunt resistance for the pre-sintered samples varies over a wide range but is almost always 2 $k\Omega cm^2$ or greater. As can be seen from Tables I and II, the trend is for series resistance and contact resistance to increase with sintering temperature and for shunt resistance to decrease. The values of contact resistance and shunt resistance after sintering at 400°C are still quite respectable and are not expected to affect cell performance. However, the increase in series resistance to $\sim$1.0 Ωcm^2 after the 400°C sinter is significant and contributes to the degradation of fill factor and efficiency with sintering. It might be noted that the observed increase of series resistance and contact resistance with sintering temperature runs counter to a-priori expectations.

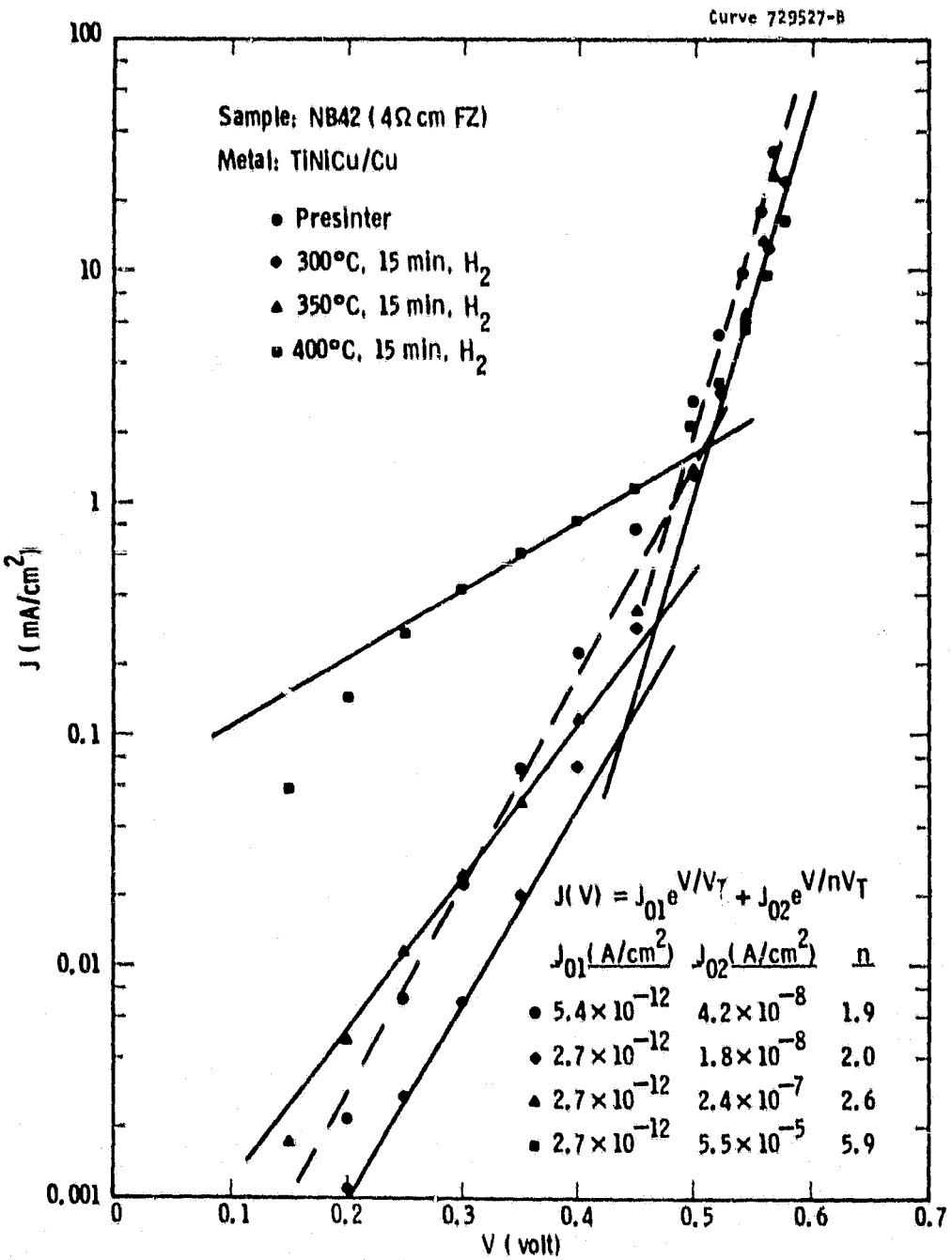

Figure 7. Effect of sintering on dark I-V characteristics for the Ti Ni Cu/Cu system.

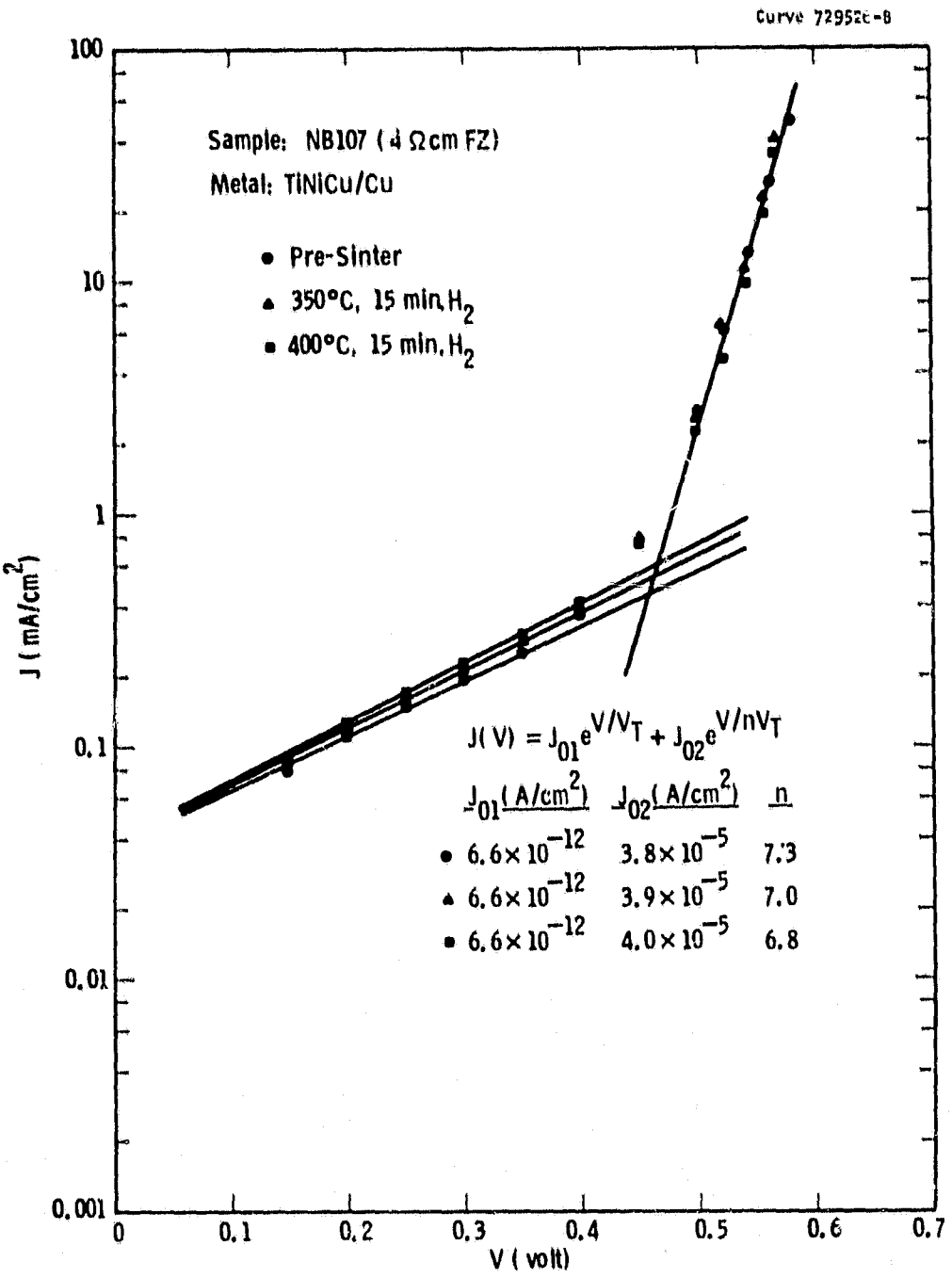

Figure 8. Effect of sintering on dark I-V characteristics for the Ti Ni Cu/Cu system.

3.1.5 Results of 300°C Sinter

As described in Section 3.1.4, cell efficiency tended to degrade with increased sintering temperature over the range 300°C to 400°C. It was therefore decided that only a mild sintering should be given to those samples having the baseline contact system or the first experimental contact system. The sintering conditions chosen were 300°C for 15 minutes in hydrogen flowing at 10 ℓ/min through a 109-mm ID tube. The test results before and after sintering for 24 samples prepared with the TiPdAg/Cu contact system are given in Table III. Similar results are given in Table IV for 27 samples prepared with the TiNiCu/Cu system.

From Tables III and IV it can be seen that good quality cells were prepared with both contact systems, since more than half the cells had efficiencies in excess of 15.0% prior to sintering. Sintering, even at 300°C, reduced cell efficiency. In those cases where efficiency was reduced by more than 2.0 % (absolute), the cells are marked with an asterisk in Tables III and IV. There were 5 such cells of the 24 total for the TiPdAg/Cu system and 1 such cell of the 27 total for the TiNiCu/Cu system. Disregarding the test results following sintering for those samples marked with an asterisk, the average efficiency dropped from 14.6% to 14.1% as a result of 300°C sintering for the TiPdAg/Cu system, and from 15.0% to 14.4% for the TiNiCu/Cu system. The degradation in efficiency was accompanied by a degradation in fill factor and open-circuit voltage. These effects could result from an increase in the junction leakage current by shunting or by increasing the number of recombination centers in the depletion region, as suggested by the dark I-V data of Section 3.1.4. Short-circuit current density and contact resistance were not significantly changed by the sintering. A few samples were checked for contact adherence after sintering by the scotch-tape peel test. In this limited test, the contacts were not separated from the silicon by the peeled tape.

3.1.6 Results of Humidity Test

In the early days of silicon solar cells, a two-layer titanium/silver contact system was used. This system was susceptible to corrosion,

TABLE III. Effect of 300°C Sintering on Cells
Having the Baseline Contact System

Material: Float Zone Silicon, Boron-doped, 4Ωcm, <111>, 250 μm thick
Evaporated: 500Å Ti, 300Å Pd, 300 Å Ag
Electroplated: 5 μm Cu
Cell Size: (1.60 x 4.00) cm
Test Conditons: 91.6 mW/cm^2, AM1, Room Temperature
Note: For each sample, the first line gives cell parameters prior to sintering amd the second line gives cell parameters after sintering at 300°C for 15 min in H_2 at 10 ℓ/min

Run	Sample	J_{sc} (mA/cm^2)	V_{oc} (V)	FF	η(%)	τ_{ocd} (μsec)	R_c (μΩcm^2)
N-4	NB93	31.2	0.583	0.789	15.7	8.4	-
	NB93	30.6	0.561	0.779	14.6	7.2	-
N-4	NB96	31.2	0.581	0.781	15.5	9.9	-
	NB96	30.6	0.560	0.769	14.4	5.8	-
N-4	NB98	31.1	0.572	0.770	15.0	10.4	-
	NB98	30.2	0.548	0.763	13.8	3.0	-
N-4	NB99	31.1	0.572	0.777	15.1	9.4	-
	*NB99	30.4	0.401	0.431	5.7	2.5	-
N-5	NB115	30.2	0.567	0.785	14.7	0.2	2.5
	NB115	30.6	0.550	0.766	14.0	-	-
N-5	NB116	29.8	0.561	0.783	14.3	6.0	2.9
	NB116	29.9	0.544	0.773	13.7	3.4	-
N-5	NB117	29.4	0.548	0.783	13.8	0.1	3.4
	NB117	29.5	0.532	0.761	13.0	0.1	-
N-5	NB119	29.7	0.568	0.786	14.5	3.6	4.3
	NB119	29.9	0.550	0.754	13.6	2.6	-
N-5	NB120	30.0	0.575	0.793	14.9	3.9	3.0
	NB120	30.4	0.559	0.768	14.2	0.6	-
N-5	NB121	29.9	0.572	0.793	14.8	6.5	1.2
	*NB121	30.2	0.547	0.625	11.3	0.2	-

TABLE III - continued

Run	Sample	J_{sc} (mA/cm^2)	V_{oc} (V)	FF	η(%)	τ_{ocd} (μsec)	R_c (μΩcm^2)
N-5	NB124	30.0	0.577	0.796	15.1	10.7	1.6
	NB124	30.6	0.562	0.770	14.4	6.8	-
N-5	NB125	29.8	0.572	0.790	14.7	5.5	1.4
	*NB125	30.0	0.554	0.686	12.5	3.1	-
N-8	NB164	27.9	0.579	0.794	14.0	13.7	9.0
	NB164	30.7	0.567	0.780	14.8	7.8	7.5
N-8	NB167	30.4	0.568	0.790	14.9	6.8	3.5
	NB167	30.7	0.553	0.783	14.5	4.9	3.1
N-8	NB168	27.9	0.574	0.793	13.8	6.5	2.9
	NB168	30.8	0.564	0.756	14.4	1.8	3.5
N-8	NB171	30.6	0.575	0.791	15.2	6.8	-
	NB171	30.9	0.563	0.760	14.5	1.3	-
N-8	NB174	30.8	0.580	0.797	15.5	11.7	8.7
	NB174	31.2	0.566	0.775	15.0	1.4	9.1
N-8	NB175	30.5	0.577	0.805	15.5	4.7	19.1
	NB175	30.9	0.563	0.784	14.9	0.5	12.7
N-10	NB218	30.2	0.588	0.794	15.4	10.4	3.3
	*NB218	30.2	0.571	0.692	13.0	0.1	5.0
N-10	NB219	30.4	0.585	0.791	15.4	9.8	2.6
	NB219	30.5	0.573	0.768	14.7	0.3	3.4
N-10	NB220	30.2	0.581	0.789	15.1	8.4	3.9
	NB220	30.4	0.569	0.772	14.6	1.7	5.4
N-10	NB221	30.1	0.586	0.798	15.4	8.3	3.1
	NB221	30.1	0.571	0.777	14.6	0.3	5.7
N-10	NB222	30.8	0.587	0.787	15.5	0.6	3.1
	*NB222	30.8	0.568	0.690	13.2	0.3	3.0
N-10	NB223	30.3	0.588	0.794	15.5	10.9	8.1
	NB223	30.2	0.572	0.785	14.8	0.5	6.8

*Denotes those cells whose efficiency fell by more than 2% absolute after sintering at 300°C.

TABLE IV. Effect of 300°C Sintering on Cells
Having the First Experimental Contact System

Material: Float Zone Silicon, Boron-doped, 4 Ωcm, <111>, 250 μm thick
Evaporated: 500Å Ti, 400 Å Ni, 300 Å Cu
Electroplated: 5 μm Cu
Cell Size: (1.60 x 4.00) cm
Test Conditions: 91.6 mW/cm^2, AM1, Room Temperature
Note: For each sample, the first line gives cell parameters prior to sintering and the second line gives cell parameters after sintering at 300°C for 15 min. in H_2 at 10 ℓ/min

Run	Sample	J_{sc} (mA/cm^2)	V_{oc} (V)	FF	η(%)	τ_{ocd} (μsec)	R_c (μΩ.cm^2)
N-4	NB85	30.8	0.576	0.788	15.3	4.2	-
	NB85	30.2	0.547	0.779	14.1	8.4	-
N-4	NB87	31.2	0.586	0.790	15.8	11.0	-
	NB87	30.6	0.562	0.778	14.6	11.0	-
N-4	NB89	31.7	0.583	0.783	15.8	7.2	-
	NB89	31.0	0.561	0.772	14.7	4.2	-
N-4	NB92	31.1	0.572	0.762	14.8	10.4	-
	NB92	30.5	0.548	0.753	13.7	4.7	-
N-5	NB103	26.7	0.508	0.736	10.9	3.0	-
	NB103	28.7	0.504	0.656	10.4	1.8	-
N-5	NB106	27.9	0.518	0.774	12.2	2.8	1.6
	NB106	27.8	0.504	0.750	11.5	2.6	-
N-5	NB108	29.7	0.542	0.770	13.5	2.7	7.5
	NB108	29.5	0.536	0.756	13.0	2.3	-
N-5	NB109	30.0	0.551	0.787	14.2	1.1	-
	NB109	29.9	0.542	0.766	13.6	0.5	-
N-5	NB110	29.5	0.539	0.770	13.4	1.2	2.9
	NB110	29.3	0.529	0.740	12.5	0.9	-
N-5	NB111	29.3	0.545	0.778	13.6	4.9	1.3
	NB111	29.3	0.535	0.765	13.1	3.6	-

Table IV - continued

Run	Sample	J_{sc} (mA/cm^2)	V_{oc} (V)	FF	n(%)	τ_{ocd} (usec)	R_c (μΩ.cm^2)
N-5	NB112	28.7	0.538	0.775	13.1	5.5	4.6
	NB112	28.9	0.526	0.759	12.6	5.5	-
N-5	NB113	30.0	0.571	0.775	14.5	6.2	4.7
	*NB113	29.2	0.563	0.601	10.8	1.6	-
N-8	NB152	31.0	0.591	0.787	15.8	8.1	3.1
	NB152	30.7	0.575	0.788	15.2	8.3	3.0
N-8	NB153	30.6	0.586	0.801	15.7	11.7	1.6
	NB153	30.8	0.571	0.786	15.1	8 4	1.6
N-8	NB155	28.2	0.584	0.783	14.0	15.0	1.1
	NB155	30.9	0.573	0.763	14.7	14.3	1.0
N-8	NB158	30.7	0.585	0.794	15.6	18.0	0.1
	NB158	31.1	0.570	0.778	15.0	16.2	0.8
N-8	NB159	28.2	0.583	0.795	14.3	8.4	5.2
	NB159	31.0	0.573	0.777	15.1	7.8	4.9
N-8	NB160	30.7	0.586	0.793	15.6	19.8	1.5
	NB160	30.9	0.572	0.773	14.9	10.4	1.6
N-8	NB161	30.7	0 575	0.794	15.3	12.3	1.6
	NB161	30.8	0.560	0.783	14.7	15.0	1.4
N-8	NB163	30.7	0.581	0.800	15.6	19.5	3.5
	NB163	30.7	0.568	0.788	15.0	15.0	3.3
N-10	NB205	30.8	0.588	0.796	15.7	12.5	-
	NB205	30.5	0.587	0.777	15.2	7.8	-
N-10	NB206	30.2	0.587	0.797	15.4	3.0	3.5
	NB206	30.4	0.579	0.773	14.9	3.1	4.1

Table IV - continued

Run	Sample	J_{sc} (mA/cm^2)	V_{oc} (V)	FF	n(%)	τ_{ocd} (μsec)	R_c (μΩ.cm^2)
N-10	NB207	30.3	0.584	0.786	15.2	5.3	3.0
	NB207	30.4	0.579	0.768	14.8	4.7	3.4
N-10	NB208	29.9	0.583	0.801	15.2	4.2	3.9
	NB208	29.9	0.567	0.803	14.8	4.4	4.3
N-10	NB209	30.5	0.589	0.795	15.6	13.3	3.9
	NB209	30.2	0.576	0.769	14.6	14.6	4.2
N-10	NB210	30.0	0.582	0.794	15.2	5.6	4.4
	NB210	29.6	0.573	0.779	14.4	3.4	5.3
N-10	NB211	29.4	0.581	0.797	14.9	13.3	-
	NB211	29.1	0.570	0.780	14.1	14.3	-

* Denotes those cells whose efficiency fell by more than 2% absolute after sintering at 300°C.

however, as a galvanic action was set up between the titanium and the silver even under very modest humidity conditions. In the titanium/silver couple, titanium is anodic. It was found that this couple could be passivated by separating the titanium and silver with a thin layer of palladium.[12] This was demonstrated by Fischer & Gereth by subjecting both Ti/Ag and TiPd/Ag contact systems to a 100% relative humidity 90°C test. After 36 hours under these conditions, the Ti/Ag system had blistered and the Ag could easily be separated. The TiPd/Ag system (350Å Ti, 50-200Å Pd, 5 μm Ag), however, was unaffected even after 600 hours under these conditions. Later, the TiPd/Ag system was qualified for space solar cells and became the industry standard.

By way of comparison with the space cell contact system, in our first experimental contact system the palladium layer is replaced by nickel and the conductive silver layer is replaced by copper. Since copper comes from the same group as silver in the Periodic Table and nickel comes from the same group as palladium, one might suspect that the TiNiCu/Cu system would be chemically similar to the TiPd/Ag system and would, therefore, also be corrosion resistant. This was checked by subjecting both the baseline contact system (TiPdAg/Cu) and the first experimental contact system (TiNiCu/Cu) to a humidity test. The test conditions were 85% relative humidity at 85°C for 100 hours.

The results of the humidity test are given in Tables V and VI. For the baseline contact system of Table V there are five samples, three of which had been sintered at 300°C and two of which had not. Four of the samples were unaffected by the test, while one sample (NB168) suffered a significant decrease in fill factor and efficiency. A similar group of samples with the first experimental contact system was tested. As can be seen from Table VI, these samples were not degraded by the humidity test. The results of this test indicate, then, that the TiNiCu/Cu system is not susceptible to corrosion.

TABLE V. Effect of Humidity on Cells
Having the Baseline Contact System

Material: Float Zone Silicon, Boron-doped 4 Ωcm, <111>, 250 μm thick
Contact System: 500 Å Ti, 300 Å Pd, 300 Å Ag/5 μm Cu
Cell: (1.60 x 4.00) cm tested at 91.6 mW/cm^2, AM1, Room Temperature
Humidity Test Conditions: 85% Relative Humidity, 85°C for 100 hours
Note: For each sample, the first line gives cell parameters prior to the humidity test and the second line gives cell parameters following the humidity test.

Sample	J_{sc} (mA/cm^2)	V_{oc} (V)	FF	η(%)	τ_{ocd} (μsec)	R_s (Ω.cm^2)	R_{sh} (kΩ.cm^2)	R_c (μΩ.cm^2)
NB164	30.7	0.567	0.780	14.8	7.8	–	–	7.5
	30.8	0.586	0.745	14.7	3.4	0.61	93.	8.6
*NB165	30.8	0.568	0.795	15.2	9.8	–	–	7.0
	30.7	0.590	0.792	15.6	4.1	0.62	3.6	7.0
*NB166	30.8	0.562	0.790	15.0	8.3	–	–	5.4
	30.8	0.582	0.786	15.4	9.1	0.81	10.	5.7
NB167	30.7	0.553	0.783	14.5	4.9	–	–	3.7
	30.8	0.573	0.761	14.6	2.1	0.81	2.0	3.6
NB168	30.8	0.564	0.756	14.4	1.8	–	–	3.5
	30.8	0.579	0.623	12.1	0.3	0.72	15.	8.4

* Sample not sintered prior to humidity test; all others were sintered at 300°C for 15 minutes in H_2 at 10 ℓ/min prior to humidity test.

TABLE VI. Effect of Humidity on Cells Having the First Experimental Contact System

Material: Float Zone Silicon, Boron-doped 4 Ωcm, <111>, 250 μm thick
Contact System: 500 Å Ti, 400 Å Ni, 300 Å Cu/ 5 μm Cu
Cell: (1.60 x 4.00) cm tested at 91.6 mW/cm^2, AM1, Room Temperature
Humidity Test Conditions: 85% Relative Humidity, 85°C for 100 hours
Note: For each sample, the first line gives cell parameters prior to the humidity test and the second line gives cell parameters following the humidity test

Sample	J_{sc} (mA/cm^2)	V_{oc} (V)	FF	η(%)	τ_{ocd} (μsec)	R_s (Ω.cm^2)	R_{sh} (kΩ.cm^2)	R_c (μΩ.cm^2)
NB152	30.7	0.575	0.788	15.2	8.3	–	–	3.0
	30.6	0.588	0.781	15.4	5.8	0.78	7.7	3.3
NB153	30.8	0.571	0.786	15.1	8.4	–	–	1.6
	30.7	0.586	0.773	15.2	5.5	0.65	8.1	2.0
*NB154	30.8	0.568	0.776	14.8	8.4	–	–	3.6
	30.7	0.585	0.773	15.1	8.4	0.78	16.	4.2
NB155	30.9	0.573	0.763	14.7	14.3	–	–	1.0
	31.0	0.589	0.739	14.7	15.0	1.20	5.7	1.3
*NB157	31.0	0.568	0.785	15.1	9.1	–	–	4.3
	31.0	0.584	0.783	15.5	11.0	0.74	4.7	4.9

* Sample not sintered prior to humidity test; all others were sintered at 300°C for 15 minutes in H_2 at 10 ℓ/min prior to humidity test.

3.1.7 Results of Accelerated Aging Test

In order to obtain at least a qualitative idea of the stability of the TiNiCu/Cu system compared to the TiPdAg/Cu system, an accelerated aging test was carried out. Five samples from each contact system were subjected to 250°C for 250 hours in air. When the samples were removed from the oven at the conclusion of the test, the metallic surface was blackened. This was presumed to be copper oxide and was removed in a solution of 4 parts (by volume) water and 1 part concentrated hydrochloric acid.

The results of the test are given in Tables VII and VIII, where it is seen that the TiNiCu/Cu system behaved in a similar fashion to the TiPdAg/Cu system. For both systems the cell efficiency decreased because of a deterioration of the junction quality, as reflected by a drop in the fill factor. There was little change in the short-circuit current, which indicates that the bulk of the cell was not affected by the test. These results are similar to those obtained from the 300°C sinter (Tables III and IV).

Of the five TiNiCu/Cu samples, two had not been sintered and three had been sintered at 300°C prior to the test. The efficiency of the unsintered samples decreased by 1.1% (absolute) while the efficiency of the sintered samples decreased by 0.04%. Similarly, for the TiPdAg/Cu samples, two had not been sintered and their efficiency decreased by 1.9% (absolute) while three had been sintered and they suffered an efficiency loss of 1.0%. As a general conclusion, it can be stated that the TiNiCu/Cu samples withstood the accelerated aging test at least as well as the TiPdAg/Cu samples.

3.1.8 Ultrasonic Bonding of Aluminum Interconnects to Nickel-Coated Cell Pad

Making reliable ultrasonic bonds between the aluminum interconnect strip and the cell contact pad requires that the metal surface of the pad be clean and not highly oxidized. In addition, it is desirable that the surface metal on the cell pad and the metal of the interconnect strip have only a small difference in electrochemical potential so that the propensity toward corrosion is correspondingly small. For these reasons, samples of both the baseline and the first experimental contact systems were prepared with

TABLE VII. Effect of Accelerating Aging Test on Cells Having the Baseline Contact System

Material: Float Zone Silicon, Boron-doped 4 Ω cm, <111>, 250 μm thick
Contact System: 500 Å Ti, 300 Å Pd, 300 Å Ag/5 μm Cu
Cell: (1.60 x 4.00) cm tested at 91.6 mW/cm^2, AM1, Room Temperature
Accelerated Aging Test Conditions: 250°C for 250 hours in air
Note: For each sample, the first line gives cell parameters prior to the accelerated aging test and the second line gives cell parameters following the test.

Sample	J_{sc} (mA/cm^2)	V_{oc} (V)	FF	η(%)	τ_{ocd} (μsec)	R_s (Ω.cm^2)	R_{sh} (kΩ.cm^2)	R_c (μΩ.cm^2)
*NB129	30.2	0.575	0.799	15.2	11.0	–	–	0.9
	29.8	0.575	0.742	13.9	10.4	0.77	85.	1.6
*NB214	30.6	0.586	0.789	15.4	15.6	–	–	13.1
	30.5	0.576	0.676	13.0	2.1	0.92	64.	17.8
NB215	29.9	0.577	0.782	14.7	0.1	–	–	5.2
	29.2	0.584	0.705	13.1	0.3	0.61	7.2	12.7
NB219	30.5	0.573	0.768	14.7	0.3	–	–	3.4
	30.1	0.583	0.708	13.6	5.8	0.76	3.3	3.4
NB220	30.4	0.569	0.772	14.6	1.7	–	–	5.4
	30.3	0.582	0.746	14.4	7.8	0.79	88.	7.9

* Sample not sintered prior to accelerated aging test; all others were sintered at 300°C for 15 minutes in H_2 at 10 ℓ/min prior to accelerated aging test.

TABLE VIII. Effect of Accelerated Aging Test on Cells Having the First Experimental Contact System

Material: Float Zone Silicon, Boron-doped 4 Ωcm, <111>, 250 μm thick
Contact System: 500 Å Ti, 400 Å Ni, 300 Å Cu/ 5 μm Cu
Cell: (1.60 x 4.00) cm tested at 91.6 mW/cm^2, AM1, Room Temperature
Accelerated Aging Test Conditions: 250°C for 250 hours in air
Note: For each sample, the first line gives cell parameters prior to the accelerated aging test and the second line gives cell parameters following the test

Sample	J_{sc} (mA/cm^2)	V_{oc} (V)	FF	η(%)	τ_{ocd} (μsec)	R_s (Ω.cm^2)	R_{sh} (kΩ.cm^2)	R_c (μΩ.cm^2)
*NB202	30.0	0.589	0.803	15.5	5.7	-	-	2.7
	30.2	0.587	0.723	14.0	5.7	0.86	17.	7.9
*NB203	30.1	0.582	0.797	15.2	15.1	-	-	14.3
	29.9	0.580	0.774	14.6	19.5	0.70	5.8	16.7
NB209	30.2	0.576	0.769	14.6	14.6	--	-	4.2
	30.0	0.584	0.754	14.5	14.6	0.47	42.	4.5
NB210	29.6	0.573	0.779	14.4	3.4	-	-	5.4
	29.6	0.578	0.769	14.4	3.6	0.81	14.	5.2
NB211	29.1	0.570	0.780	14.1	14.3	-	-	-
	29.0	0.580	0.774	14.2	15.0	0.65	17.	8.2

* Sample not sintered prior to accelerated aging test; all others were sintered at 300°C for 15 minutes in H_2 at 10 ℓ/min prior to accelerated aging test.

an additional plated top layer of nickel to give TiPdAg/Cu/Ni and TiNiCu/Cu/Ni structures. Aluminum interconnects were then ultrasonically bonded to the nickel-coated cell pads and the strengths of the bonds were determined by pull testing.

The nickel layer was deposited on the copper surface of the cell contacts by electroplating using the commercial SEL REX LECTRO-NIC 10-03 plating bath and a de-skinned rolled carbon nickel anode. The four-liter bath was agitated by a magnetic stirrer, and the temperature and pH were in the range 125-135°F and 2.4 - 4.0, respectively. A plating current of 200 mA for 5 minutes was used to plate the entire back as well as the exposed metal surface on the front of the 2-inch wafer (see Fig. 4a). This gives a nickel layer the thickness of which is estimated to be 2 μm.

The electrical test results for five samples prepared in this way are given in Table IX. Aluminum interconnects, 1.5 mils thick, were then bonded to the nickel-coated cell contact pads. Pull tests on 24 bonds were then made, with the pull force being directed either in the plane of the cell or perpendicular to that plane. In all 24 cases, the aluminum interconnect yielded before the aluminum could separate from the nickel in the bonded area. The aluminum fingers yielded at 150 - 220 g-force. Since the bond area is 0.010 cm^2, this indicates that the bonds themselves can withstand a stress greater than 213 to 312 psi. Thus, a nickel coating could be used as the surface contact metal to protect the underlying copper and provide a base to which strong bonds can be made to the aluminum interconnects.

3.1.9 Nickel-Copper Contact System - Background

Nickel has several attractive features as a contact metal for solar cells. Such a contact might be expected to be adherent if Ni_2Si is formed by sintering at a relatively low temperature. Nickel is said to act as a barrier to prevent copper from diffusing into the silicon and destroying the cell. It is possible, but by no means trivial, to plate nickel onto silicon so that the entire contact system (nickel and copper) may be plated. This would permit the elimination of any metal evaporation step in the process. Finally, the nickel and copper metals used in such a system are relatively inexpensive.

TABLE IX. Nickel Deposition on Copper as a Protective Coating

Material: Float Zone Silicon, 4 Ωcm, < 111>, 250 μm thick
Metal System:

1. Evaporate 500Å Ti, 300 Å Pd, 300 Å Ag; Plate 5 μm Cu, 2 μm Ni
2. Evaporate 500 Å Ti, 400 Å Ni, 300 Å Cu, Plate 5 μm Cu, 2 μm Ni

Heat Treatment: None
Cell Size: 1.60 x 4.00 cm

ID	Metal System	J_{sc}	V_{oc}	FF	η
NB94	1	29.3 mA/cm^2	0.579V	0.783	14.5%
NB95	1	29.6	0.582	0.778	14.6
NB97	1	29.5	0.584	0.782	14.7
NB88	2	30.1	0.587	0.764	14.7
NB91	2	28.3	0.534	0.772	12.8

Some idea of the effectiveness of nickel as a diffusion barrier to copper can be obtained by extrapolating high temperature diffusion data to the lower temperatures that are typical of solar cell operating conditions. From data giving the diffusion constant for copper into nickel over the temperature range 840 - 1400°C,[13] an Arrhenius-type relation was constructed. This relation is:

$$D_{Cu \to Ni} = D_o \, e^{-E_a/kT} \qquad (16)$$

where $D_o = 1.95$ cm^2/sec and $E_a = 2.84$ eV. Equation 16 can be used to estimate the depth of penetration of Cu into Ni under typical contact sintering conditions or under solar cell operating conditions. A contact sintering at 350°C gives $D_{Cu \to Ni}(T = 623°K) = 2.1 \times 10^{-23}$ cm^2/sec. A characteristic diffusion length for a sintering time of 30 minutes is computed as $\sqrt{Dt} = 0.03$ Å. Similarly, the penetration of copper into nickel over a 20-year life at 45°C is estimated to be much less than 1Å from Equation 16.

These estimates indicate that nickel will act as an effective diffusion barrier for copper in solar cell applications. However, it is not known exactly how the samples were prepared or analyzed in the diffusion study on which Equation 16 is based. If Equation 16 represents the kinetics of diffusion of copper into bulk nickel, then it may grossly underestimate the extent to which copper will diffuse along grain boundaries in a fine-grained nickel film, as in an evaporated nickel film. In addition, an extrapolation of the diffusion constant from 840°C to 350°C or 45°C, as was done above, must be viewed with some skepticism.

The growth kinetics of Ni_2Si on <100> silicon wafers has been studied.[14] Nickel films of 1300 Å or 2000 Å thickness were electron-beam evaporated onto the silicon substrate at a rate of 50 Å/sec. The predeposition vacuum was 5×10^{-6} Torr. The samples were heat treated both in high-purity helium and in a vacuum of 5×10^{-6} Torr over a temperature range 200°C to 325°C. The Ni_2Si phase was found to form over this temperature range, and it was determined that Ni diffuses through the Ni_2Si layer to the Si substrate in order to form additional Ni_2Si. The thickness of the Ni_2Si layer was found to increase as the square root of time at a constant temperature. This indicates that the rate of formation of Ni_2Si is limited by the diffusion of Ni through the Ni_2Si rather than by the rate of the reaction of Ni and Si.

In another study[15] the stress in thin nickel silicide films was measured as a function of temperature. In this case a 520 Å Ni film was electron-beam evaporated onto a <111> silicon substrate and annealed in a vacuum of approximately 10^{-5} Torr. The film stress was found to vary systematically and abruptly over the temperature range 200°C to 350°C. This temperature range agrees with the range over which Ni_2Si was formed in the previous study.

The effect of orientation of the silicon substrate on the kinetics of Ni_2Si formation was also investigated.[16] It was determined that Ni_2Si forms on <111>-oriented silicon substrates over the temperature range 200°C to 325°C, but only at one-quarter the rate of formation on <100>-oriented substrates. In this work Ni films of 1000 Å to 5000 Å thickness were electron-beam evaporated on the Si substrates. During evaporation a vacuum of 7×10^{-7} Torr was maintained. Annealing was done for 1/2 - 24 hours in a vacuum of 7×10^{-7} Torr. Nuclear backscattering was used to show that Ni_2Si thickness increased as the square root of time for a constant temperature. From the data given,[16, 17] an expression is constructed relating the thickness of the Ni_2Si layer (d) to the heat-treatment temperature (T) and time (t) for <111>-oriented silicon substrates. This relation is:

$$d = (7.23 \times 10^{9} \text{ Å} / \sqrt{\text{hr}}) \sqrt{t}\, e^{-0.8 \text{ eV}/kT} \qquad (17)$$

and is valid for Ni_2Si formed on <111> silicon over the temperature range 200°C to 350°C. From Equation 17, the thicknesses of Ni_2Si formed as a result of heat treatment for 1/2 hour at 200°C, 250°C, 300°C, and 350°C are estimated to be 15 Å, 100 Å, 470 Å, and 1720 Å, respectively.

A nickel-copper contact system has been developed for solar cell contacts and subjected to some thermal stress testing.[18] In one such test, samples of a solar cell contact were prepared by depositing ~ 5000 Å of Ni on Si by electroless plating. The samples were then heat treated at 250°C for 30 minutes in a nitrogen atmosphere. From Equation 17, this heat treatment is expected to yield a 120 Å thick Ni_2Si layer if the silicon substrate is <111>-oriented or a 400 Å thick layer if the substrate is <100>-oriented. On one sample the unreacted Ni was etched leaving only the thin Ni_2Si layer, and no etching of the Ni was done for a second sample. Both samples were then copper plated and subjected to a temperature stress of 300°C for 15 minutes. It was found that the first solar cell with the Ni_2Si/Cu contact was severely

degraded while the second solar cell with the Ni_2Si/Ni/Cu contact was not affected. Further stressing of the second solar cell at 300°C for an additional 45 minutes did not alter the cell-lighted I-V curve. However, an increase in the low-current segment of the dark I-V curve, associated with increased shunting or junction recombination current, was noted. The general conclusion from this work was that a layer of Ni, approximately 5000 Å thick, is a suitable diffusion barrier for Cu at 300°C, but a presumed thin layer of Ni_2Si, perhaps 100 - 400 Å thick, is not.

3.1.10 Nickel-Copper Contact System -- Experimental Results.

In an attempt to evaluate the effectiveness of nickel as a diffusion barrier to copper and to examine the characteristics of a nickel-copper contact system for solar cells, a number of samples was prepared. This is the second experimental contact system and typically consists of an evaporated layer of nickel and a plated layer of copper. The nickel layer was deposited by electron-beam evaporation of 99.99% pure nickel at a rate of 20 Å/sec. Prior to nickel deposition, the evaporator system was pumped to a vacuum of $\sim 1 \times 10^{-6}$ Torr. The thickness of the nickel layer was either 600 Å or 1200 Å.

In preparing solar cell samples, the process sequence outlined in Section 3.1.3 was used except, of course, that nickel was evaporated in Step 7. However, it was not possible to obtain good adherence between the electroplated copper and the evaporated nickel using the standard acid sulfate copper plating bath. This bath is composed of 187 g/ℓ of copper sulfate ($CuSO_4 \cdot 5H_2O$) and 21 mℓ/ℓ of concentrated sulfuric acid (H_2SO_4). The plating current is 10 mA/cm^2 with the bath at room temperature.

In order to provide a surface which could be plated using the acid sulfate-copper plating bath, two different approaches were taken. In the first approach, a 300 Å layer of copper was deposited on the 600 Å or 1200 Å nickel layer during the evaporation step. It was then possible to plate copper onto this evaporated-copper layer to give a Ni Cu/Cu structure. In the second approach, a thin "strike" layer of copper was plated onto the evaporated-nickel surface using an alkaline cyanide plating bath. This bath was made by combining 26 g/ℓ of CuCN, 34 g/ℓ of NaCN, and 30 g/ℓ of $Na_2CO_3 \cdot 10H_2O$ with the appropriate amount of deionized water. A sufficient quantity of NaOH was

then added to bring the pH into the range 12.0 to 12.6. The copper strike layer was plated at 1.2 mA/cm^2 for one minute with the plating bath in the temperature range 54°C to 71°C. Presumably, this alkaline cyanide bath was able to reduce the oxide that had formed on the evaporated nickel so that a good nickel-copper bond could be made. The required thickness of copper (5 μm) was then built up by plating on the "strike" copper surface using the acid sulfate copper bath. This approach then gave a Ni/Cu/Cu structure.

Solar cells of (1.60 x 4.00) cm size were prepared with this second experimental contact system (NiCu/Cu or Ni/Cu/Cu) using float zone silicon, as before. These cells were then heat treated at temperatures ranging from 250°C to 400°C for 30 minutes in flowing nitrogen. Test results both before and after heat treatment, are given in Table X. The column labeled "Metal" in Table X refers to the layers of metal that were evaporated or, in the case of sample NB184, sputtered onto the silicon. It is understood that those samples having only Ni under the "Metal" column received a strike layer of copper from the alkaline cyanide bath before being plated using the acid sulfate bath.

From Table X it can be seen that prior to heat treating, the 12 samples have good junction characteristics with average values of -9.3 for Log (J_o) and 1.14 for N, and an average efficiency of 13.0%. Heat treatment, however, causes cell degradation, especially at temperatures of 350°C and above. The efficiency decreases by 0.3% (absolute) after the 250°C treatment, decreases by 0.2% after the 300°C treatment (if sample NB186, which had poor contact adherence, is ignored), decreases by 3.0% after the 350°C treatment, and decreases by 8.7% after the 400°C treatment. In all cases, the decrease in efficiency is accompanied by an increase in the junction parameters Log (J_o) and N and a corresponding decrease in fill factor. The implication is that either nickel or copper or perhaps both are diffusing into the vicinity of the junction and are degrading the cell.

Contact adherence was tested after heat treatment by the Scotch-tape peel test for one sample in each of the four groups of Table X. Some contact grid lines were lifted by the tape in each case, with typically 5 of 14 grid lines being dislodged. This suggests that Ni_2Si, if formed, did not act as a strong bond between the nickel and the silicon as expected.

TABLE X. Effect of Heat Treatment on Cells Having the Second Experimental Contact System

Material: Float Zone Silicon, Boron-Doped 4Ω-cm, <111>, 250 μm thick
Evaporated (Sputtered): 600 Å or 1200 Å Ni, as noted, and 300 Å Cu in some cases
Electroplated: 5μm Cu
Cell Size: (1.60 x 4.00) cm_2
Test Conditions: 91.6 mW/cm^2, AM1, Room Temperature
Heat Treatment: Temperature as noted, 30 minutes in N_2
Note: For each sample, the first line gives the cell parameters prior to heat treatment and the second line gives the parameters after heat treatment.

Sample	Metal	J_{sc} (mA/cm^2)	V_{oc} (V)	FF	η(%)	Log(J_o)	N	R_s (Ωcm^2)	R_{sh} ($k\Omega cm^2$)	R_c ($\mu\Omega cm^2$)
A. Heat Treatment Temperature: 250°C										
NB183	600 Å Ni	29.0	0.542	0.773	13.3	-9.8	1.10	—	3.6	2.9
	300 Å Cu	29.1	0.533	0.715	12.1	-6.1	1.96	0.93	2.7	16.4
NB189	1200 Å Ni	28.5	0.510	0.769	12.2	-9.4	1.09	—	4.4	<0.1
		28.3	0.525	0.748	12.1	-7.8	1.41	0.60	4.3	0.7
NB194	1200 Å Ni	29.3	0.515	0.771	12.7	-9.2	1.13	—	7.9	4.1
	300 Å Cu	29.0	0.539	0.759	13.0	-8.2	1.34	0.42	4.3	3.8
B. Heat Treatment Temperature: 300°C										
NB177	600 Å Ni	27.9	0.505	0.780	12.0	-9.6	1.05	—	—	2.2
		27.6	0.512	0.753	11.6	-7.9	1.34	0.58	9.2	3.3
NB181	600 Å Ni	30.2	0.546	0.771	13.9	-8.8	1.25	—	—	4.4
	300 Å Cu	30.0	0.557	0.763	13.9	-8.7	1.30	—	1.4	4.5
NB186	1200 Å Ni	29.0	0.521	0.771	12.7	-8.2	1.30	—	—	7.9
		28.7	0.445	0.400	5.6	-6.1	1.62	6.98	0.6	27.2
C. Heat Treatment Temperature: 350°C										
NB182	600 Å Ni	29.6	0.537	0.771	13.9	-8.8	1.25	—	—	7.2
	300 Å Cu	29.1	0.532	0.550	9.3	-3.1	5.68	0.68	4.0	12.3

Sample	Metal	J_{sc} (mA/cm^2)	V_{oc} (V)	FF	η(%)	Log(J_o)	N	R_s (Ωcm^2)	R_{sh} (kΩcm^2)	R_c (μΩcm^2)
NB187	1200 Å Ni	29.1	0.523	0.780	12.9	-9.6	1.09	—	—	3.9
		28.7	0.532	0.697	11.6	-4.8	2.72	0.70	2.1	6.6
NB192	1200 Å Ni	29.2	0.542	0.787	13.6	-9.9	1.08	—	—	28.7
	300 Å Cu	28.7	0.538	0.620	10.5	-3.0	6.21	0.73	9.0	17.7
D. Heat Treatment: 400°C										
NB178	600 Å Ni	28.2	0.514	0.784	12.4	-9.4	1.09	—	—	52.1
		26.6	0.160	0.470	2.2	-4.2	1.03	0.38	0.7	—
NB184	1200 Å Ni	28.3	0.519	0.782	12.6	-9.3	1.12	—	—	—
	(sputtered)	27.7	0.504	0.564	8.6	-2.9	6.24	0.54	0.8	—
NB193	1200 Å Ni	29.7	0.537	0.779	13.6	-9.8	1.08	—	—	2.9
	300 Å Cu	28.7	0.127	0.418	1.7	-3.8	0.92	0.42	0.2	1.8

In order to check for the formation of Ni_2Si and to obtain direct information on the efficacy of evaporated nickel as a diffusion barrier to copper, samples were prepared through metal evaporation in the same way that the solar cell samples were prepared. These were 2-inch boron-doped 4Ωcm float zone silicon wafers with <111> orientation, as before. They underwent phosphorous and boron diffusions and then had 1200 Å of Ni and 300 Å of Cu evaporated on both sides. No further processing was done until these samples were heat treated along with the solar cells between 250°C and 400°C for 30 minutes in flowing N_2. An elemental depth profile was then obtained for these samples by Auger Electron Spectroscopy (AES) with in-situ sputter etching. The etching was done through the evaporated metals and into the n^+ side of the silicon. The resultant profiles for a sample before heat treatment are shown in Figure 9. The transition regions in Figure 9, especially from Ni to Si, are probably artificially wide because the sputter etching is not perfectly uniform. In addition to the elements shown, the surface of all samples (including those which have been heat treated) contain ∿ 7 atomic percent chlorine and ∿ 25 atomic percent carbon.

Figures 10, 11, 12, and 13 give the corresponding elemental profiles for samples that have been heat treated at 250°C, 300°C, 350°C, and 400°C, respectively. There are two important results that are evident in Figures 10 through 13. The first result concerns the formation of Ni_2Si. This compound is clearly present in Figure 13 (400°C, 30 minutes) where it is shown that the full 1200 Å thick Ni layer has reacted to form Ni_2Si. In Figure 12 (350°C, 30 minutes) there is a shoulder in the Ni profile and in the Si profile which may indicate the initiation of a Ni_2Si layer which is perhaps 200 Å thick. The Ni profile in Figure 11 (300°C, 30 minutes) has a slight discontinuity in slope near the Ni/Si interface which suggests the onset of Ni_2Si formation. No hint of Ni_2Si formation appears in Figure 10 (250°C, 30 minutes). These thicknesses of Ni_2Si are less than anticipated from Equation 17, which gives Ni_2Si thicknesses of 100 Å, 470 Å, 1720 Å, and 5330 Å for a 30-minute heat treatment at 250°C, 300°C, 350°C, and 400°C, respectively.

The second result from Figures 10 through 13 concerns the penetration of copper into the nickel layer. The profiles of Figures 10, 11, and 12 indicate that copper is nearly uniformly present throughout the

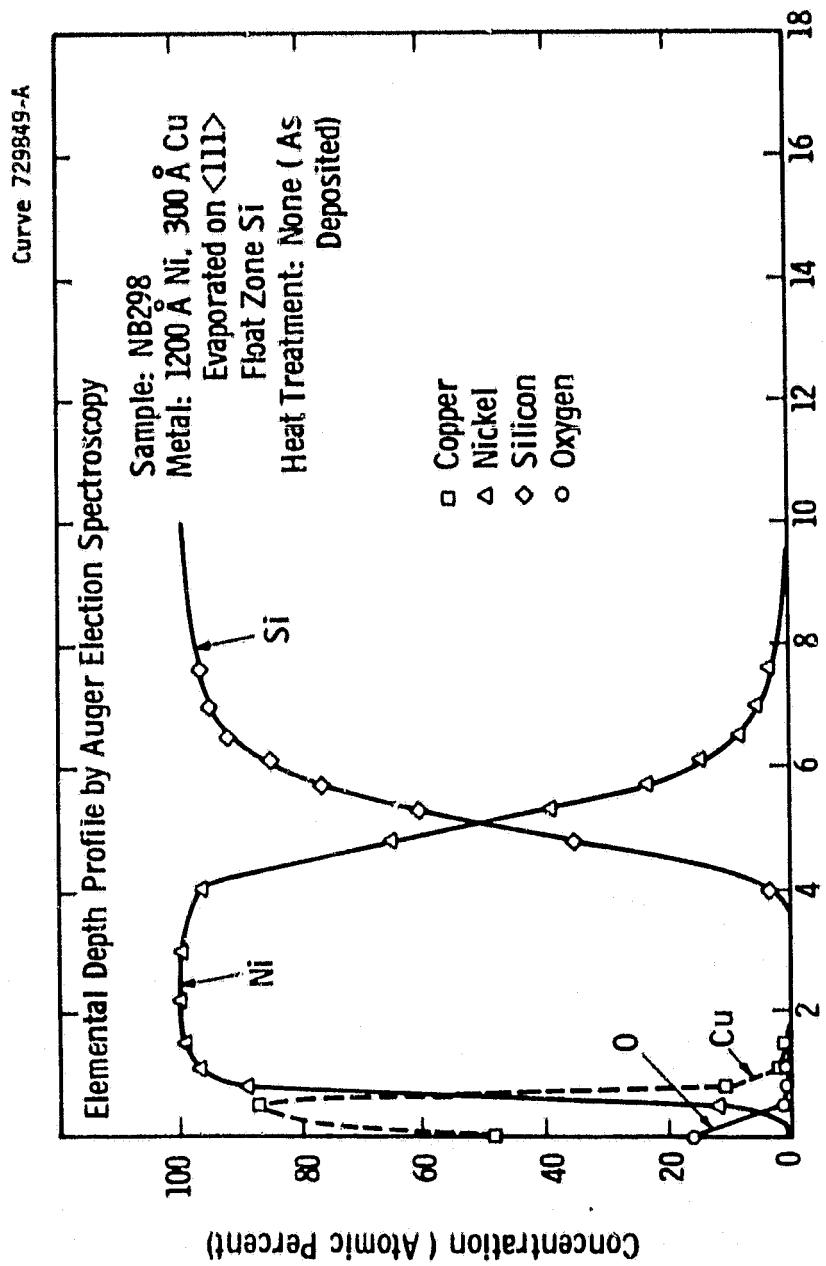

Figure 9. AES elemental depth profile for the NiCu system as deposited.

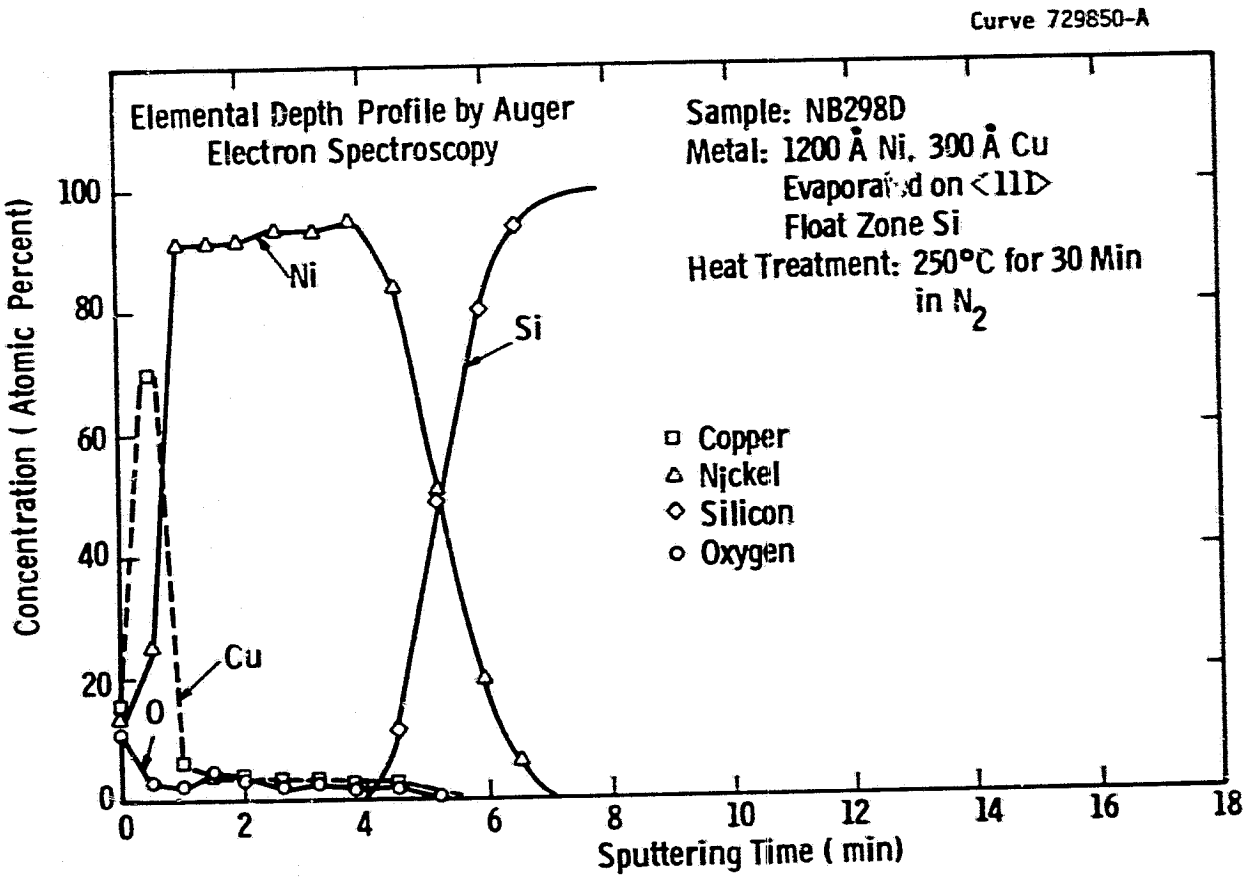

Figure 10. AES elemental depth profile for the NiCu system after heat treatment at 250°C for 30 minutes in N_2.

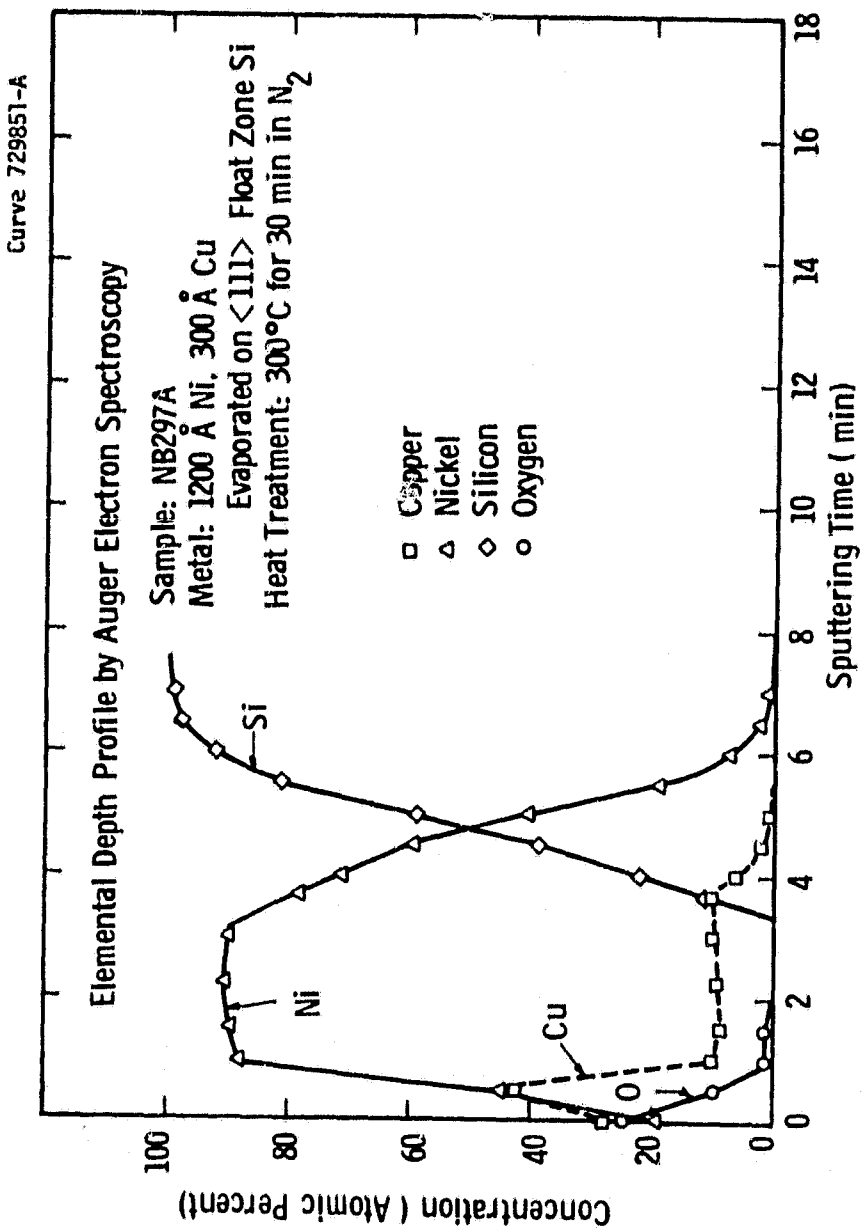

Figure 11. AES elemental depth profile for the NiCu system after heat treatment at 300°C for 30 minutes in N_2.

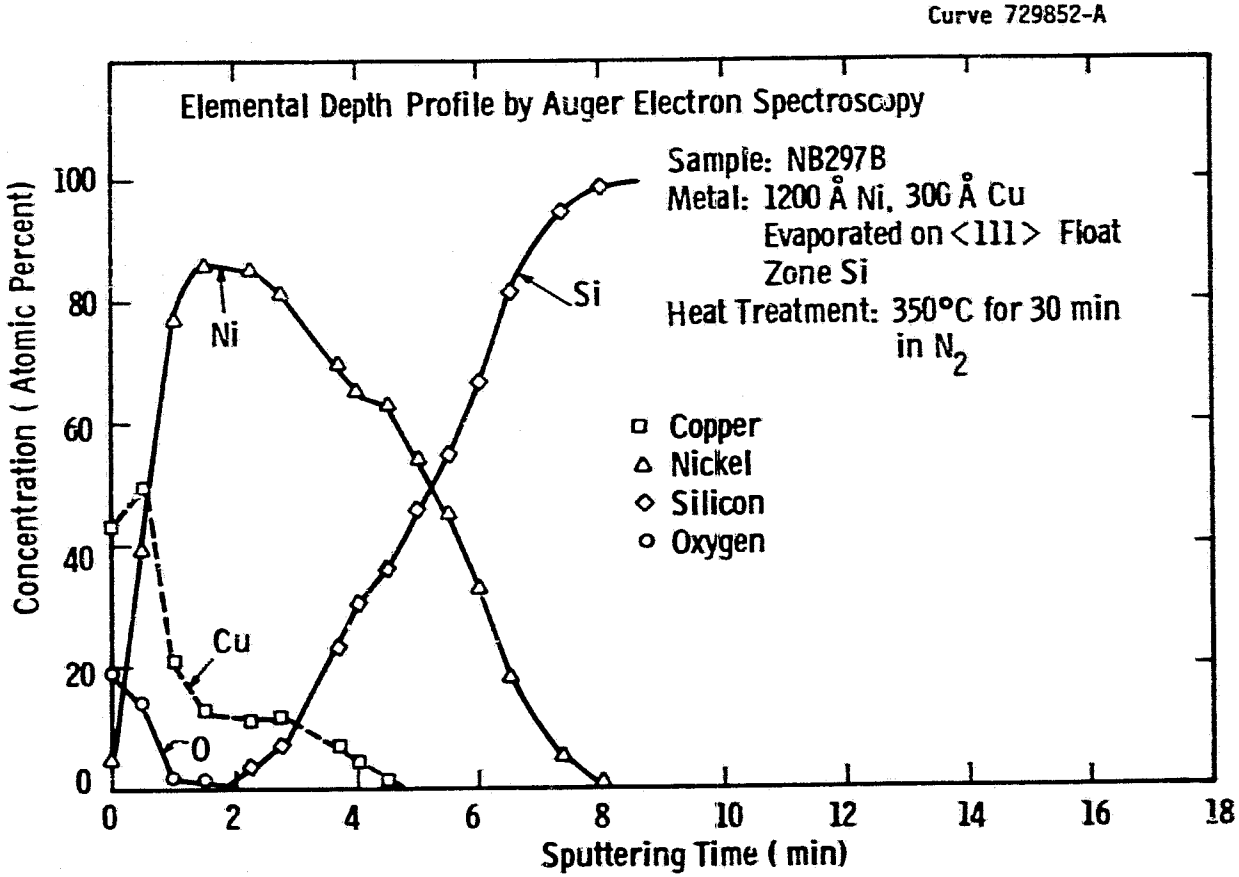

Figure 12. AES elemental depth profile for the NiCu system after heat treatment at 350°C for 30 minutes in N_2.

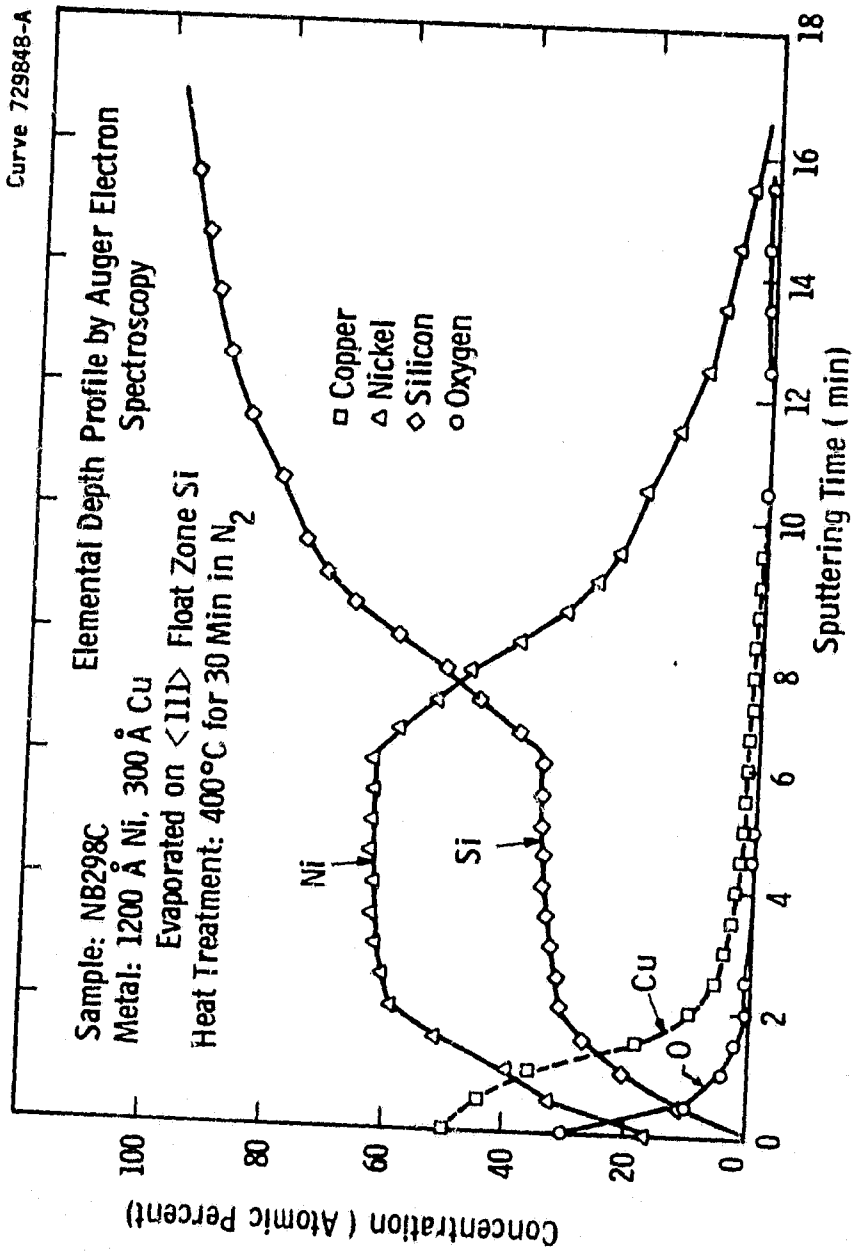

Figure 13. AES elemental depth profile for the NiCu system after heat treatment at 400°C for 300 minutes in N_2.

nickel layer. The amount of copper present in the nickel increases with heat-treatment temperature and is 5 atomic percent at 250°C, 10 atomic percent at 300°C, and 12 atomic percent at 350°C. In addition to the fact that nickel does not act as a barrier to copper at these temperatures, another surprising aspect of these profiles is that the copper concentration does not decrease with depth into the nickel layer as one would expect for a typical complementary error-function diffusion profile. Rather, the copper concentration profile tends to be flat throughout the nickel layer. Because of this flat copper profile, it is not meaningful to assume a complementary error-function distribution and extract from these data a diffusion constant for the diffusion of copper in nickel.

These results of Figures 10, 11, and 12 suggest that evaporated-nickel films of $\sim$ 1200 Å thickness perform quite poorly as a diffusion barrier to copper over the temperature range 250°C to 350°C. This agrees with recent work[19] in which nuclear backscattering on vacuum-deposited Cu/Ni bilayers is used to show that strong interdiffusion sets in at 400°C after annealing for 15 minutes. Other recent work[20] contends that the performance of solar cells having an (electroless) nickel-copper metallization system will not be degraded over a 20-year lifetime provided the cell, assumed to operate 6 hours/day, is not regularly heated above 120°C while operating. In that work it was assumed that cell degradation was a result of nickel diffusing into the junction region of the silicon, rather than copper diffusing through the nickel. It was also shown there that V_{oc} at room-light illumination ($\sim$ 5 mW/cm^2) began to decrease after a temperature stress test of 4-10 hours at 250°C or 20 minutes at 300°C. This drop was taken to be a precursor of observable cell deterioration.

In Figure 13, copper is seen to have completely penetrated the Ni_2Si layer at 400°C. This suggests that Ni_2Si is also not a diffusion barrier to copper at this temperature. This statement cannot be made with certainty, however, because it is not known whether the copper first mixed with the nickel before a significant amount of Ni_2Si was formed or whether the Ni_2Si layer formed and then copper diffused through it.

In an attempt to monitor the formation of Ni_2Si, the sheet resistance of an evaporated-nickel film on the large (1.27 cm) square of Figure 4A was measured as a function of time at a fixed temperature. As a typical case, a 600 Å nickel film was evaporated on the n+ diffused silicon substrate. The

substrate had a sheet resistance of $\sim$ 60 Ω/□ and the measured sheet resistance of the film on the substrate was 2.17 Ω/□. This corresponds to a resistivity of the evaporated nickel of 13.0×10^{-6} Ωcm, which is approximately twice as high as the resistivity of bulk nickel (6.8×10^{-6} Ωcm). It is common for evaporated films to have a higher resistivity than their bulk counterparts because the evaporated films are very fine-grained.

If Ni_2Si is formed, then the sheet resistance will change. Although the resistivity of Ni_2Si was not found in the literature, the resistivity of high-temperature silicide phases varies from 12 μΩcm for WSi_2 to 914 μΩcm for $CrSi_2$, with $NiSi_2$ having a resistivity of 118 μΩcm.[21] When the sample described above with a 600 Å nickel film was heat treated at 350°C in flowing nitrogen, the sheet resistance changed only slightly from 2.17 Ω/□, as deposited, to 2.32 Ω/□ after 10 minutes, 2.15 Ω/□ after 40 minutes, and 2.25 Ω/□ after 100 minutes. These changes are considered to be very minor and suggest that no significant quantity of Ni_2Si was found, unless the resistivity of Ni_2Si happens to be nearly the same as the resistivity of the evaporated-nickel film. Similar results were obtained for other samples which were heat treated at 300°C.

X-ray diffraction was also used to examine five samples that had been heat treated for evidence of Ni_2Si. Two samples had undergone heat treatment at 350°C for 100 minutes in flowing nitrogen and three samples had been heat treated at 300°C for either 24 minutes or 95 minutes in flowing hydrogen. No diffraction peaks associated with Ni_2Si were observed for any of the samples, although strong peaks were detected for nickel, silicon, and copper (when present).

The failure to detect Ni_2Si by sheet resistance or X-ray diffraction measurements suggests that at least in some cases, Ni_2Si is not formed. This failure occurs in spite of the fact that the heat-treatment temperature (250°C - 350°C) and time (30 minutes - 120 minutes) fall within the appropriate range for Ni_2Si formation. A possible explanation for this is that the silicon surface may not have been properly cleaned prior to evaporation so that a barrier prevented the reaction of nickel and silicon at these relatively low temperatures. (The standard cleaning is a 10-second dip in 10:1 H_2O:HF just before loading the samples into the evaporator.) To check this possibility, several samples were loaded into a sputtering system, and $\sim$ 100Å of silicon was sputter etched in vacuum to remove any possible surface contamination.

A nickel film was then sputtered onto the silicon without breaking the vacuum. The samples were then heat treated at 350°C for 100 minutes in flowing nitrogen. The resultant elemental profiles, both for the film as deposited and after heat treatment, are given in Figure 14. There it is seen that even in this case there is no appreciable amount of Ni_2Si formed.

This result prompts one to inquire further as to why Ni_2Si is not being formed. It seems that the most likely answer is that the nickel film is being contaminated either during evaporation or during heat treatment with something that prevents nickel and silicon from coming in contact so they can react. Recent work[22] has shown that the growth of nickel silicides can be greatly altered by the presence of impurities. If a few atomic percent of oxygen is present in the nickel film, then this oxygen is able to react with the silicon during heat treatment to form SiO_2. This oxide layer then acts as a barrier to prevent formation of Ni_2Si. As can be seen from Figure 14, oxygen is present at a level of approximately 10 atomic percent in the sputtered-nickel films. However, Figure 9 shows that oxygen is not present in the evaporated nickel film at a level above 1 atomic percent.

It is instructive to estimate the flux of residual gas atoms that strike the surface during nickel evaporation. At a deposition rate of 20 Å/sec, the flux of nickel atoms is 1.8×10^{16} atoms/(cm^{2}sec). The flux of residual gas atoms depends upon residual gas pressure. Making the rough approximation that the gas is made up of diatomic molecules of mass m which strike the surface at normal incidence, the flux of residual gas atoms on the surface being metallized is:

$$\Phi \gtrsim p/2\sqrt{5mkT} \qquad (18)$$

With $p = 1 \times 10^{-6}$ Torr, T = 300°K, and m the mass of an O_2 molecule, the residual gas flux is estimated to be $\Phi \gtrsim 2.0 \times 10^{14}$ molecules/(cm^2 sec). This says that for every 90 Ni atoms that are deposited, one residual gas molecule strikes the surface being metallized. This one residual gas molecule may or may not become embedded in the evaporated-Ni layer, but this estimate points out the necessity of evaporating only under conditions of good vacuum, with 1×10^{-6} Torr of pressure or less.

The atmosphere used during heat treatment is also an object of concern. Typically, flowing nitrogen was used, but nitrogen has been shown

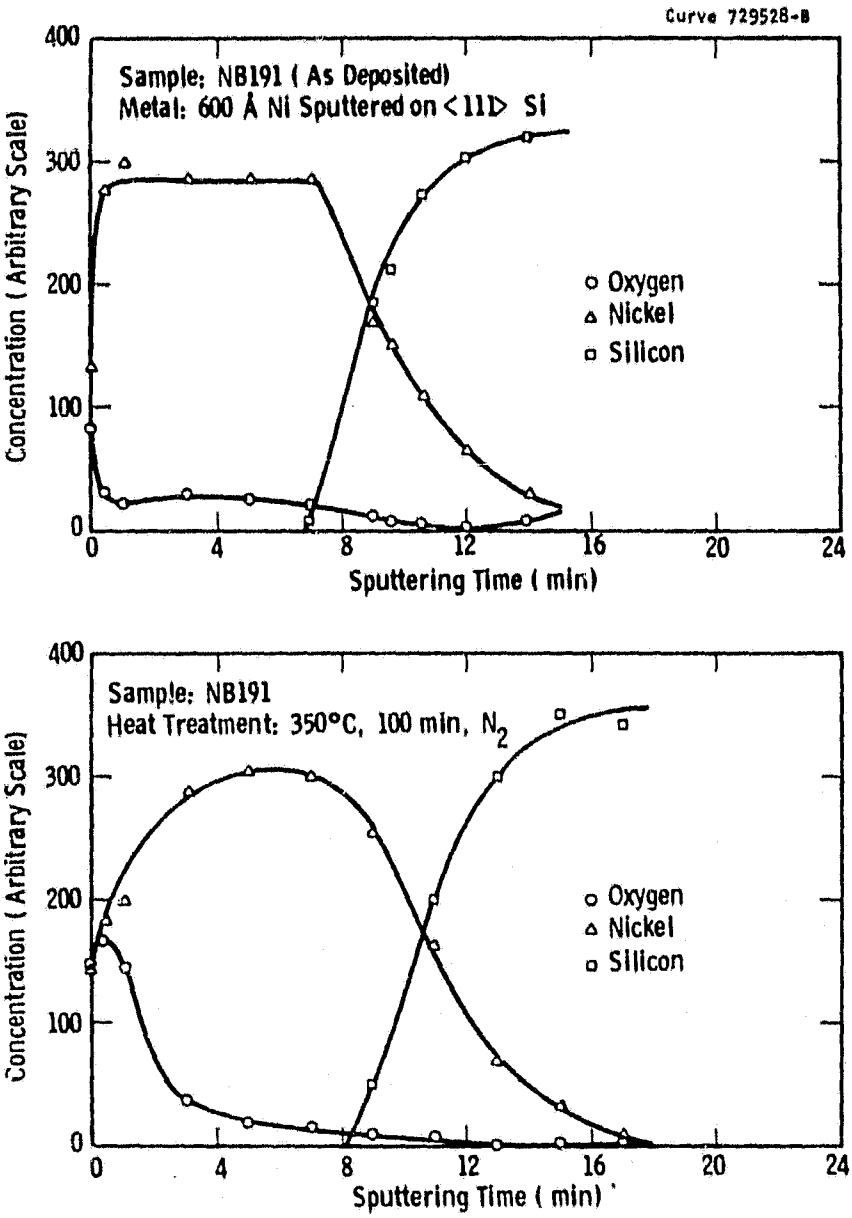

Figure 14. Elemental depth profile by Auger election spectroscopy for nickel sputtered on silicon (before and after heat treatment).

to be capable of halting the reaction between Ni and Si below 375°C if it is present in the nickel film in sufficient quantity.[22] The proposed mechanism is the formation of a silicon nitride barrier at the Ni/Si interface. A few samples were heat treated at 300°C in flowing hydrogen for up to 95 minutes, but these samples also failed to indicate Ni_2Si formation. Perhaps the heat treatment should be done in vacuum,[14,15,16] as discussed in Section 3.1.9, for best results.

3.1.11 SAMICS Cost Analysis for Candidate Contact Systems

An estimate of the cost in 1980 dollars for the contact systems investigated in this work was made using the SAMICS methodology. It was assumed that the production line would operate for 3 shifts/day and 345 days/year (4.97×10^5 minutes/year). The material costs were taken to be \$38/lb for Ti, \$896/lb for Pd, \$120/lb for Ag, \$10/lb for Ni, and \$4/lb for Cu. The analysis shows a drop of ∿ \$0.10/watt if either of the experimental contact systems is used instead of the baseline systems. This drop is attributed mostly to the elimination of Pd in the experimental contact systems. In the case of 25 mW/year production, the drop from \$0.176/watt for the baseline system to \$0.076/watt for the first experimental system is significant (see Table XI).

3.2 Fabrication of Modules

Three modules were fabricated using dendritic web silicon. The first two modules were of nominal (30 x 60) cm size and the third module was of nominal (38 x 120) cm size. In all cases the cells were interconnected by ultrasonic seam bonding and laminated using ethylene vinyl acetate.

3.2.1 Cell Data, Construction, and Test Results for the First Module

3.2.1.1 Cell Fabrication

A total of 133 cells of dimension 2.0 cm x 10.0 cm were fabricated using single crystal silicon grown by the dendritic web process. The silicon web was boron-doped and the resistivity of the material used had an average and standard deviation of 5.4 ± 1.9 Ω cm with a range of 2.3 to 11.9 Ω cm. The length of the web strips was nominally 33 cm, with the processing of one such strip yielding three 2.0 cm x 10.0 cm cells. For the web that was used in this fabrication, the average and standard deviation of the thickness and width is 172 ± 26 μm and 2.70 ± 0.22 cm, respectively.

TABLE XI. SAMICS Cost Analysis (1980 dollars)

Contact System	Cost for 1 MW/year	Cost for 25 MW/year
1. Baseline (500Å Ti, 300Å Pd, 300Å Ag, 10 μm Cu)	$0.893/watt	$0.176/watt
2. First Experimental (500Å Ti, 400Å Ni, 300Å Cu, 10 μm Cu)	0.782	0.076
3. Second Experimental (A) (600Å Ni, 300Å Cu, 10 μm Cu)	0.781	0.075
4. Second Experimental (B) (1200Å Ni, 300Å Cu, 10 μm Cu)	0.782	0.076

Note: The 10 μm layer of Cu is electroplated and the other metal layers are evaporated.

3.2.1.2 Description of Process

Beginning with 33 cm long strips of web with surfaces as grown, the process steps may be summarized as follows:

1. Remove growth oxide from the web surface;
2. Produce an n^+ layer on both sides by a $POCl_3$ diffusion at 850°C for 35 minutes;
3. Strip deposition oxide and protect the front side (sun side) with a Silox treatment;
4. Apply aluminum to the back side by a plasma spray;
5. Form a back-surface layer of aluminum-silicon alloy by passing the strip through a vertical furnace in which the hot zone is at 850°C with a nitrogen atmosphere;
6. Remove excess (i.e., unalloyed) aluminum from the back side;
7. Remove protective oxide layer from the front side;
8. Apply an antireflective coating by dipping and baking;
9. Apply a photoresist layer by dipping and baking;
10. Expose three 2 x 10 cm grid patterns on the front of the strip, expose the entire back, and develop the photoresist;
11. Define the grid pattern by etching the antireflective coating from the exposed areas;
12. Evaporate 500 Å of titanium, 300 Å of palladium, and 300 Å of silver over the entire front and back surfaces;
13. Form the grid structure on the front by dissolving the undeveloped photoresist in acetone, thereby rejecting the excess evaporated metal;
14. Electroplate copper to a thickness of approximately 10 μm on the front grid pattern and on the back metal;
15. Sinter at 350°C for 15 minutes in a hydrogen atmosphere;
16. Define the cell border by laser scribing, then separate the cell from the surrounding material;
17. Test the 2 x 10 cm cell by a lighted I-V measurement.

3.2.1.3 Cell Data

Of the 133 (2 x 10) cm cells that were fabricated, the best cell had an efficiency (η) of 14.2%, with a short-circuit current density (J_{sc})

of 29.4 mA/cm^2, an open-circuit voltage (V_{oc}) of 0.578V, and a fill factor (FF) of 0.765. These values were determined from a lighted I-V measurement using a simulated air mass 1 solar spectrum of 91.6 mW/cm^2 intensity.

Histograms of the measured efficiency, short circuit current density, open circuit voltage and fill factor for the entire 133 cell population are shown in Figs. 15, 16, 17 and 18. Excluding those cells the parameter values of which deviate from the mean by more than 3 standard deviations, the results can be summarized as follows:

$$\eta = (12.4 \pm 0.8)\ \%\ (126\ \text{cells})$$
$$J_{sc} = (27.6 \pm 0.9)\ \text{mA/cm}^2\ (125\ \text{cells})$$
$$V_{oc} = (0.548 \pm 0.014)\ \text{V}\ (132\ \text{cells})$$
$$FF = (0.763 \pm 0.017)\ \ (123\ \text{cells})$$

3.2.1.4 Ultrasonic Bonding of Cell Interconnects

The bonding of the aluminum interconnects to the cell contacts was done with the aid of an ultrasonic seam bonder from Sonobond Corporation of West Chester, Pennsylvania. The bonder was Sonoweld Model WS-1050 with Frequency Converter WS-1050, and the bonding head was a disk which made contact with the material to be bonded over a 40-mil length. The interconnect was 1.5-mil thick annealed aluminum (alloy #1145-0) and the cell contact was a 10-μm thick copper layer electroplated on an underlying thin Ti, Pd, Ag structure.

The bonding parameters were a power of 16 watts, a weight on the bonding head of 510 g, and a linear speed of the head of 0.22 inch/sec. With these parameters the aluminum/copper bond made on a 1-mm long copper contact pad would fail in a pull test at typically 150 grams-force. This is somewhat less than the yield stress of the unbonded aluminum which is approximately 200 grams-force. Since the bond area is 0.010 cm^2, 150 grams-force corresponds to 213 psi.

The electrical termination at the ends of the strings was made by bonding the 1.5-mil aluminum interconnect to a length of 1.5-mil copper foil. This bonding required a greater weight in the bonding head and a slower speed. The parameters were a power of 16 watts, a weight of 1510 grams, and a linear speed of approximately 0.1 inch/sec.

Curve 725319-A

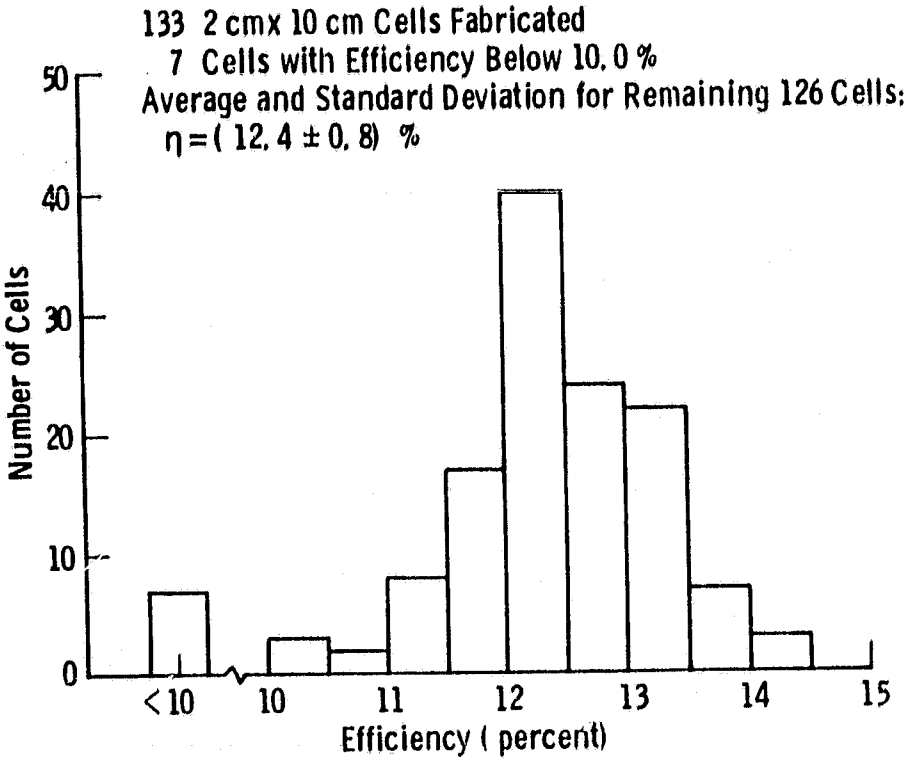

Figure 15. Efficiency histogram.

Curve 725322-A

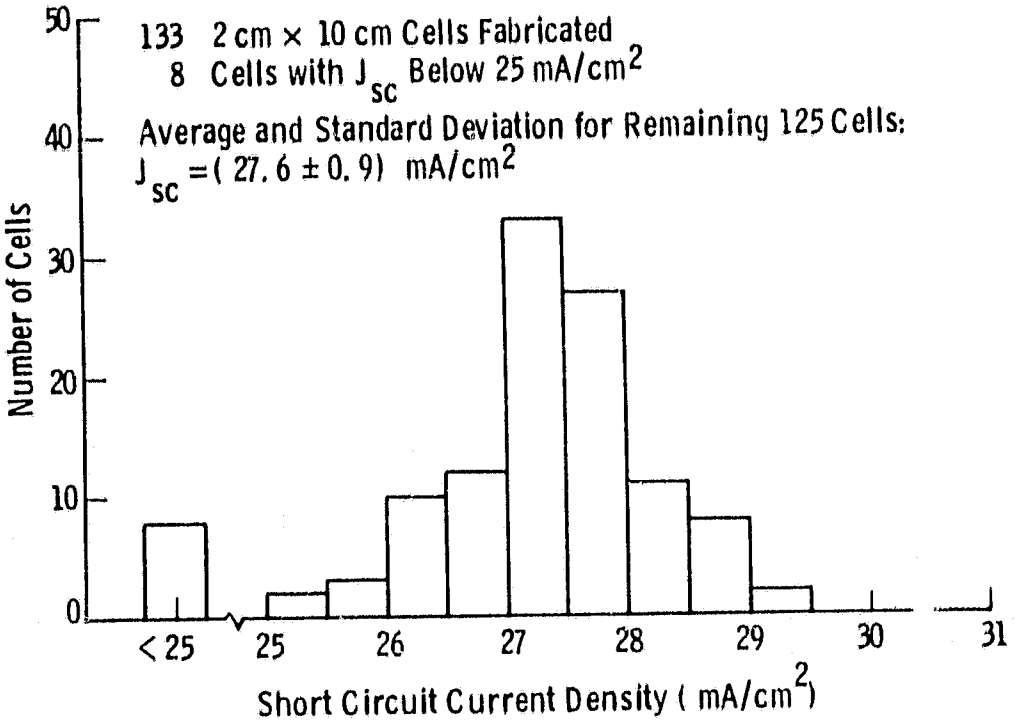

Figure 16. Short-circuit current density histogram.

Curve 725321-A

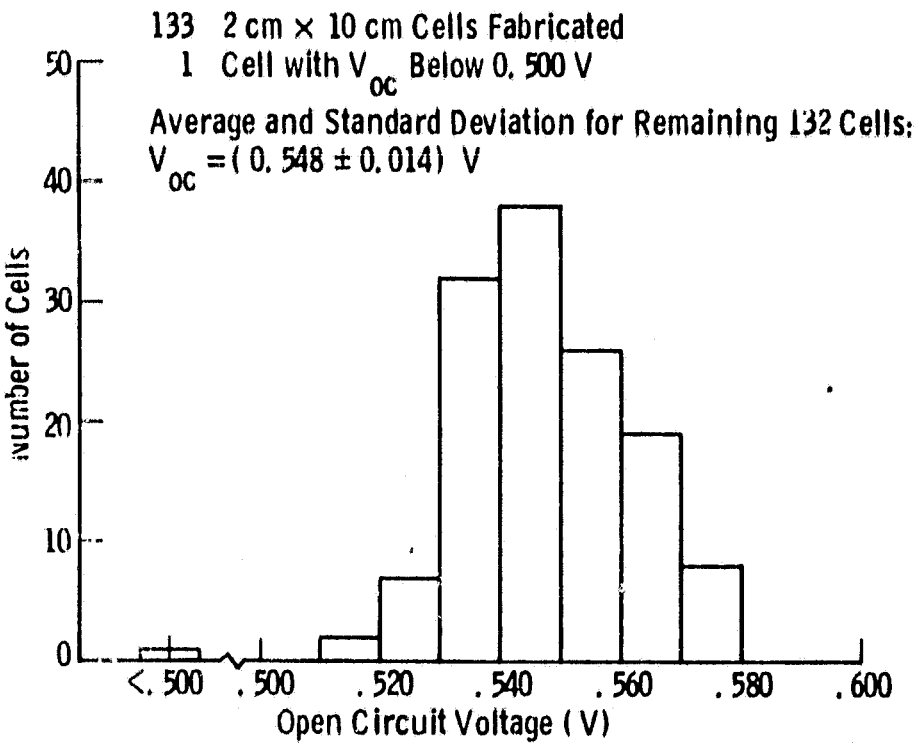

Figure 17. Open-circuit voltage histogram.

Curve 725320-A

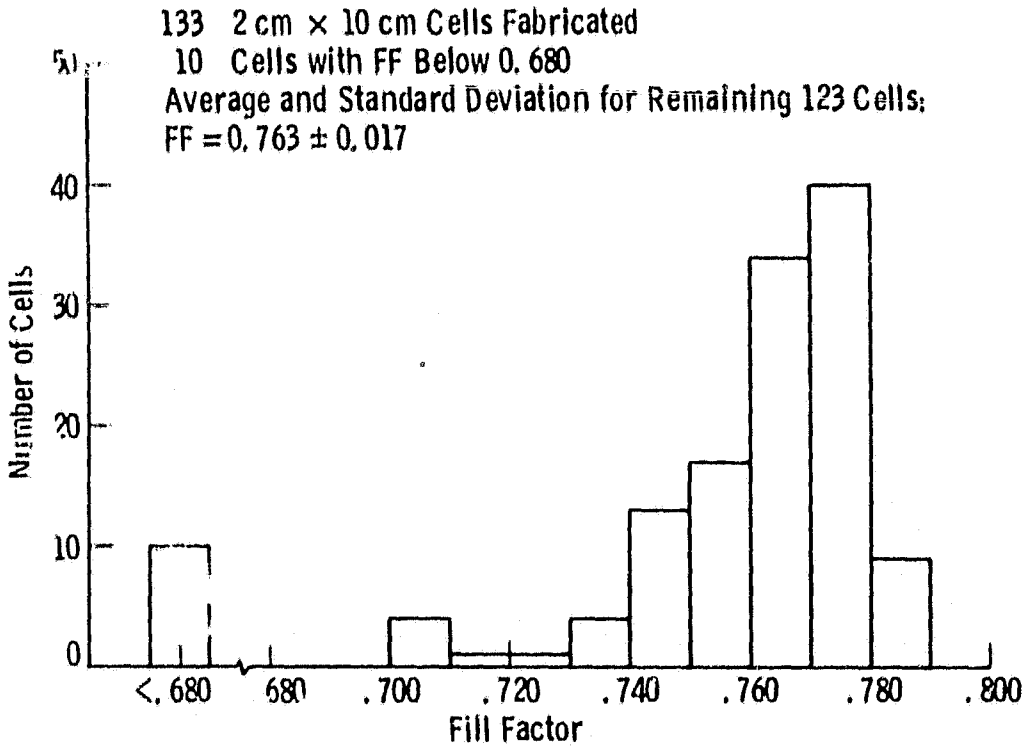

Figure 18. Fill factor histogram.

3.2.1.5 Mechanical Configuration for the First Module

The cells were laminated in the module assembly using a vacuum-bag type of lamination fixture with a Capran 80 diaphragm. The materials used in the module layup are as follows:

1. Glass: 3/16" Herculite Tempered Float Glass from Pittsburgh Plate Glass
2. Ethylene Vinyl Acetate: 17 mils
3. Cells: 7 mils
4. Craneglass : 5 mils
5. Ethylene Vinyl Acetate: 17 mils
6. Korad 212: 3 mils

After lamination, connectors (Amp #774) were soldered to the copper foil contacts which passed out of the lamination assembly. The connector housings were then epoxied to the Korad 212 using 3M epoxy EC-3501 parts A and B. This epoxy has a pot life of about 20 minutes and cured in one hour at room temperature.

An aluminum frame was then placed around the laminated assembly. The frame was designed so that the edges of the laminated assembly could be sealed with a polysulfide-modified epoxy. This modified epoxy was composed of 10 parts Shell 828 epoxy, 10 parts Thiokol LP-3 polysulfide, and 1 part Miller-Stevenson DMP-30 catalyst. The frame added 3/4 inch to both the length and the width of the module. This means that 8.8% of the module area is taken up by the frame.

3.2.1.6 Test Results for the First Module

The electrical configuration for the module is three independent strings, with each string composed of 29 (2 x 10) cm cells connected in series. The three strings could then be connected in series or in parallel externally.

The module was taken to NASA-Lewis Research Center in Cleveland, Ohio, for testing. Test conditions were an air mass 1 spectrum, 100 mW/cm^2 intensity, and the data were corrected to a temperature of 28°C. The test results for the three individual strings are given in Figure 19. The three strings are comparable in performance, but string 1 is the best with a short-circuit current of 0.496A (24.8 mA/cm^2), an open-circuit voltage of 16.08V (0.554V/cell), a peak power of 5.83W, a fill factor of 0.731, and an

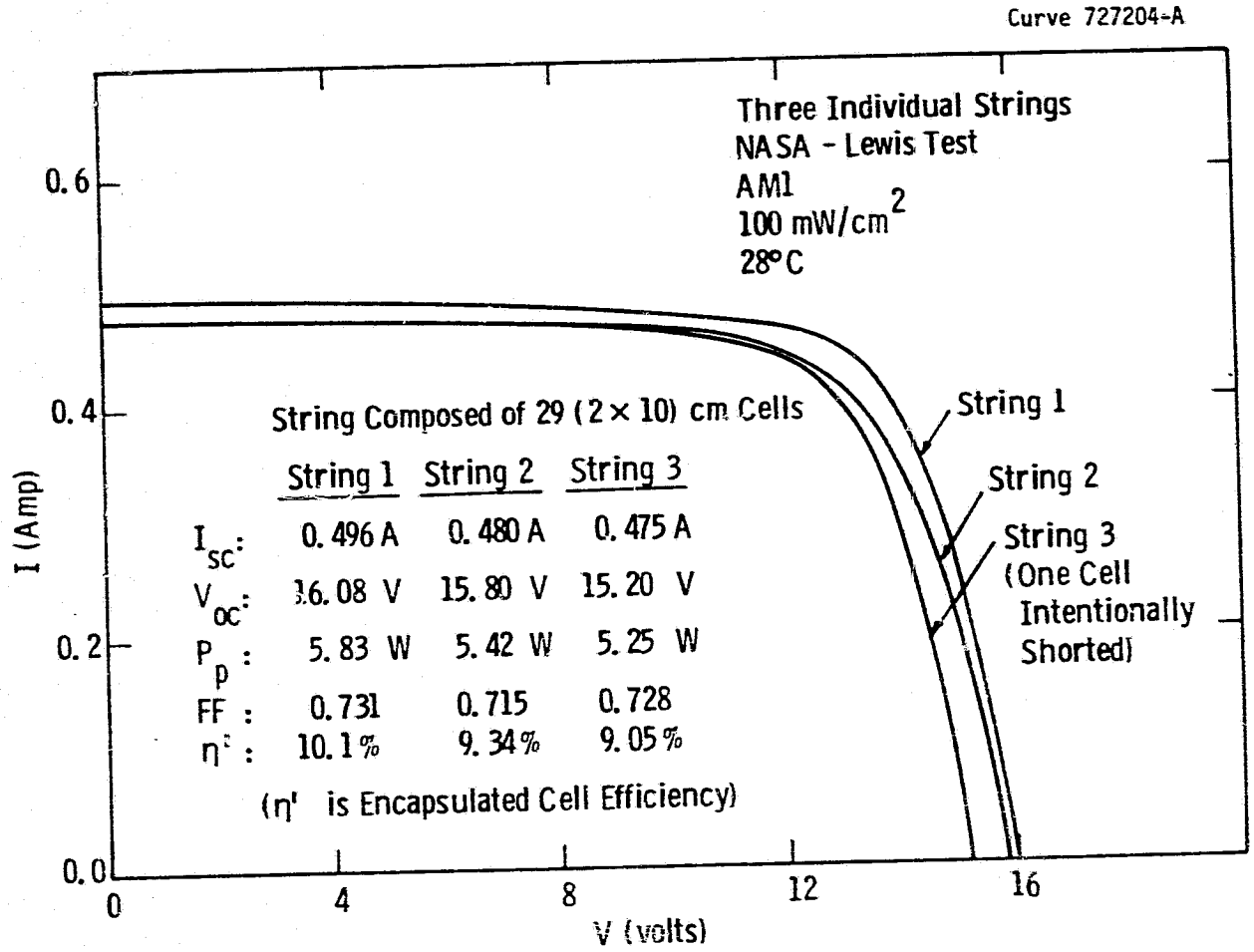

Figure 19. Lighted I-V curves for the three individual strings in the first module.

encapsulated-cell efficiency of 10.1%. Encapsulated cell efficiency for the string is defined as the ratio of power produced by the string to the power incident on the cell surface only. The power incident on the area between cells is not considered, so the encapsulated-cell efficiency is the efficiency that would be obtained if the cell-packing factor were 100% for the string. The encapsulated cell efficiency (∿10%) is considerably less than the average efficiency of individual cells (∿ 12.4%). This is primarily because of poor light transmission characteristics of the cover glass.

In string 3 a cell which had been cracked during bonding was found to give erratic results when string 3 was examined prior to encapsulation. For this reason the questionable cell was intentionally shorted prior to encapsulation. Consequently, string 3 had one fewer cell than did strings 1 and 2 and its open-circuit voltage is correspondingly less, as is evident from Figure 19.

When the module was tested with all three strings in series, the results shown in Figure 20 were obtained. With this configuration, the short-circuit current was 0.483A, the open-circuit voltage was 47.05V, and the fill factor was 0.729. This gave an encapsulated cell efficiency of 9.52% and a module efficiency of 7.91%. The cell packing factor was, therefore, 83% for this module. A photograph of the module is given in Figure 21.

3.2.2 Test Results for the Second Module

The second module was fabricated at the Westinghouse Advanced Energy Systems Division (AESD) and consisted of 87 (2 x 10) cm cells arranged in three independent series strings of 29 cells each. The overall dimensions of the frameless module are (30.8 x 61.5) cm, which gives a cell-packing factor of 92%. The process sequence used in making the cells was very similar to that described in Section 3.2.1.2, except that the back p^+p junction was formed by a Boron diffusion rather than by alloying aluminum. In addition, the cover glass for the second module was 1/8 inch thick tempered Sunadex (low iron) glass, which has better light transmission properties than the 3/16 inch thick PPG Herculite tempered float glass used in the first module. Again, the cells were interconnected by means of ultrasonic seam bonding and the encapsulation was done with ethylene vinyl acetate.

The electrical characteristics of the second module were measured

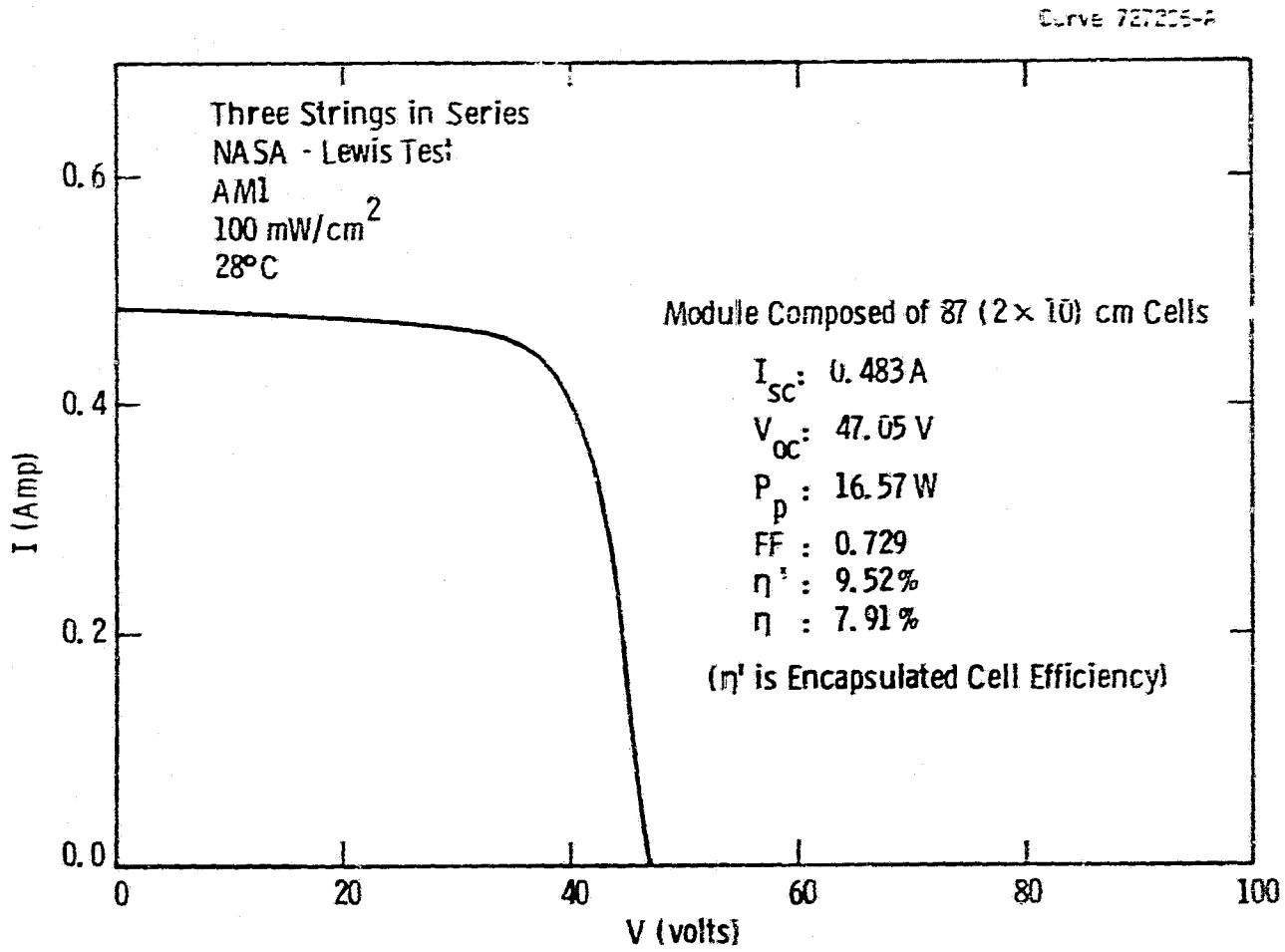

Figure 20. Lighted I-V curve for the first module with three strings in series.

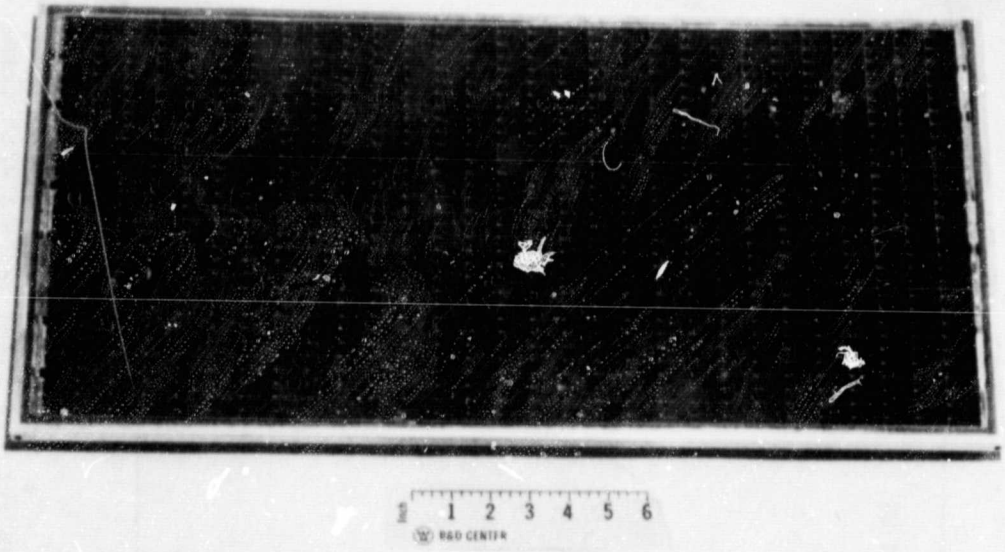

Figure 21. Photograph of module of nominal (30 x 60 cm) size.

in natural sunlight the intensity of which was near 100 mW/cm^2 Corrections were made for departure of the sunlight intensity from 100 mW/cm^2, and the data were taken in such a way that the cell temperature was ∿28°C. With the three strings connected in series, the short-circuit current was 0.508A, the open-circuit voltage was 45.4V and the fill factor was 0.724. This gave an encapsulated-cell efficiency of 9.59% and an overall module efficiency of 8.81%.

3.2.3 Test Results for the Third Module

The third module was also fabricated at the Westinghouse Advanced Energy Systems Division. Cells for this module were made using the same process sequence as was used in making cells for the second module. The cells were arranged in 12 series strings, with 17 cells/string. There were 5 strings with cells of (2.00 x 9.40) cm size and 7 strings with cells of (2.00 x 9.80) cm size. The total area covered by cells only is 3930 cm^2 and the area required by the cover glass, including a 0.5-cm border, is 4238 cm^2. The resultant packing factor for the appropriate-sized glass is 93%. Such a cover glass would have dimensions of (36.0 x 117.6) cm. However, the size of the cover glass on hand was (39.5 x 121.3) cm. For the purpose of this demonstration module, the cell strings were positioned so that a border of 0.5 cm was maintained along two edges of the cover glass. Along the other two edges the border exceeded the 0.5-cm requirement by 3.5 cm along the short edge and by 3.7 cm along the long edge. In computing module efficiency, this excess border is ignored.

As before, the cells were interconnected using ultrasonic seam bonding and the encapsulation was done with ethylene vinyl acetate. The module cover was a low-iron tempered glass the surface of which had been treated to reduce reflection losses. The module electrical characteristics were measured in natural sunlight at 95 mW/cm^2 and then were corrected to 100 mW/cm^2. The resultant values at 100 mW/cm^2 insolation are a short-circuit current of 6.83 A, an open-circuit voltage of 9.37 V, a fill factor of 0.701, an encapsulated cell (3930 cm^2) efficiency of 11.4%, and an overall module (4238 cm^2) efficiency of 10.6%.

3.3 Web Delivery

A total of 36 m of unprocessed dendritic web silicon with a minimum width of 2.5 cm was delivered to JPL. Results of test runs in which samples of the material sent to JPL were fabricated into (1 x 1) cm cells for an evaluation of web quality were also sent.

4. CONCLUSIONS

In this work the baseline contact system consists of evaporated layers of 500 Å Ti, 300 Å Pd, 300 Å Ag, and an electroplated layer of 5-μm Cu and is designated as TiPdAg/Cu. The first experimental contact system consists of evaporated layers of 500 Å Ti, 400 Å Ni, 300 Å Cu, and an electroplated layer of 5-μm Cu and is designated as TiNiCu/Cu. The second experimental contact system consists of evaporated layers of 600 Å or 1200 Å Ni, 300 Å Cu, and an electroplated layer of 5-μm Cu and is designated as NiCu/Cu. From this work the following conclusions can be drawn:

1. Both the TiPdAg/Cu system and the TiNiCu/Cu system are compatible with a high efficiency process and both have been used in fabricating (1.60 x 4.00) cm cells on float zone silicon the efficiencies of which are in excess of 15%.

2. The TiNiCu/Cu system performs at least as well as the TiPdAg/Cu system in the humidity stress test (85% RH at 85°C for 100 hours), in the accelerated aging test (250°C for 250 hours in air) and in the temperature stress test (300°C - 400°C for 15 minutes in H_2).

3. The cost of the TiNiCu/Cu system is less than the cost of the TiPdAg/Cu system by $0.100 watt. For a 25 Mw/year production capacity, changing from the TiPdAg/Cu system to the TiNiCu/Cu system would bring the cost contribution of the contact system from $0.176/watt to $0.076/watt.

4. Evaporated-Ni films of 600 Å or 1200 Å thickness are totally inadequate as diffusion barriers to Cu in the temperature range 250°C to 400°C. As a result, the long-term stability of the NiCu/Cu system is questionable.

5. The NiCu/Cu system suffers from problems of adherence between the Si and the Ni even after heat treatment, and solar cells made with this system are severely degraded by a temperature stress of 350°C for 30 minutes. The NiCu/Cu system is not a promising contact system.

6. Ultrasonic bonding for interconnecting cells and ethylene vinyl acetate for encapsulating them are suitable techniques for fabricating modules using solar cells made from dendritic web silicon, with a module efficiency of 10.6% being achieved.

5. REFERENCES

1. Coleman, M. G., et al., Motorola Inc. Semiconductor Group, Quarterly Report No. 6 for DOE/JPL Contract 954847 - 80/7, Oct. 1, 1979 to Dec. 31, 1979, pp. 22-31.

2. Van der Ziel, A., Solid State Physical Electronics, Prentice-Hall, Englewood Cliffs, NJ, 1957, p. 242.

3. Ibid., p. 252

4. Rhoderick, E. H., in Metal-Semiconductor Contacts, Conference Series Number 22, The Institute of Physics, London, 1974, M. Pepper, ed.

5. Lepselter, M. P. and J. M. Andrews, Ohmic Contacts to Semiconductors, The Elecrochemical Society, New York, NY, 1969, B. Schwartz, ed., p. 162.

6. Milnes, A. G., Semiconductor Devices and Integrated Electronics, Van Nostrand Reinhold, New York, NY, 1980, p. 99

7. Sze, S. M., Physics of Semiconductor Devices, Wiley, New York, NY, 1969, ch. 8.

8. Hopkins, R. H. et al., Seventeenth Quarterly Report on JPL Contract 954331, Jan. 1980, p. 37.

9. Smits, F. M., The Bell System Technical Journal, May, 1958, p. 711.

10. Hower, P. L. et al., Semiconductors and Semimetals, Vol. 7 Part A, Academic Press, New York, NY, 1971, Willardson, R. K. and A. C. Beer, ed., p. 147.

11. Grove, A. S., Physics and Technology of Semiconductor Devices, John Wiley & Sons, New York, NY, 1967, pp. 180-190.

12. Fischer, H., and R. Gereth, 7th IEEE Photovoltaic Specialists Conference, Pasadenn, CA, 1968, p. 70.

13. Tanner, D. P. and P. A. Iles, Optical Coating Laboratory, Inc., Third Quarterly Report for DOE/JPL Contract 955244-80/4, Oct. 15, 1979 to Jan. 15, 1980, p. 4a.

14. Tu, K. N., W. K. Chu and J. W. Mayer, Thin Solid Films, 25, 1975, p. 403

15. Koos, V. and H. G. Neuman, Physica Status Solida A., 29, 1975, p. K115.

16. Olowolafe, J. D., M. A. Nicolet and J. W. Mayer, Thin Solid Films, 38, 1976, p. 143.

17. Poate, J., K. Tu and J. Mayer, Thin Films Interdiffusion and Reactions, John Wiley and Sons, New York, NY, 1978, p. 371

18. Coleman, M. G., R. A. Pryor, T. G. Sparks, R. M. Legge, and D. L. Saltzman, Motorola, Inc., Semiconductor Group, Final Report for DOE/JPL Contract 954847-80/8, April 1, 1979 to March 31, 1980, pp. 76-84.

19. Suni, I., M. A. Nicolet and M. Maenpaa, Thin Solid Films, 79, 1981, p. 69.

20. Grenon, L. A., N. G. Sakiotis and M. G. Coleman, 15th IEEE Photovoltaic Specialists Conference, Kissimmee, Florida, 1981, p. 522.

21. Murarka, S. P., Journal of Vacuum Science and Technology, 17 (4), 1980, p. 775.

22. Wielunski, L., D. M. Scott, M. A. Nicolet and H. von Seefeld, Applied Physics Letters, 38 (2), 1981, p. 106.

6. ACKNOWLEDGMENTS

The authors gratefully acknowledge C. S. Duncan, R. G. Seidensticker and J. P. McHugh for supplying the web material; J. S. Swartz for carrying out the Auger Electron Spectroscopy measurements; R. Koznicki for performing the X-ray diffraction analysis; and J. R. Davis, A. Rohatgi and R. Mazelsky for helpful discussions. The efforts of F. S. Youngk, J. B. McNally, D. N. Schmidt, G. J. Machiko, Jr. and R. Hauser, along with personnel from the Westinghouse AESD Photovoltaic Pre-Pilot Line, in fabricating and testing the cells and modules, are also recognized. Finally, the authors would like to thank E. S. McCarty for typing this manuscript.

APPENDIX A

SPECIFICATIONS FOR PROCESS SEQUENCE USED TO FABRICATE DENDRITIC WEB SOLAR MODULES

The following describes the Westinghouse R&D process sequence and specifications used in fabricating solar cell modules from dendritic web silicon.

1. Web Cleaning

The purpose of this step is to remove the growth oxide from the web and to remove from the web surface organic and heavy metal contamination.

Process Specifications:

- Soak web in undiluted HF for 15 sec.
- If some surface oxide remains, rinse web in DI H_2O, soak in acetone and gently abrade oxide from surface while web is immersed in acetone; soak in HF again for 15 sec; rinse.
- Soak web in H_2SO_4 at 160°C $\pm$ 10°C for 4 minutes.
- Soak web in a freshly-prepared 5:1:1 solution of H_2O: H_2O_2: NH_4OH at 90 $\pm$ 10°C for 5 minutes.
- Soak web in a freshly-prepared 5:1:1 solution of H_2O: H_2O_2: HCl at 90 $\pm$ 10°C for 5 minutes.

Process Control:

Web surface is to be reflective and to have a uniform appearance.

2. Boron Diffusion

In this step, the p-type web is diffused with Boron to produce a p^+p junction which gives rise to a back surface field.

Process Specifications:

- Apply a diffusion mask of SiO_x (SILOX) of thickness 5000 $\pm$ 500 Å at 420°C to the front side of the web. (Front is side without ID number).
- Clean web with:
  - Dip in 10:1 H_2O:HF for 15 seconds.
  - Soak web in freshly prepared 5:1:1 H_2O: H_2O_2: NH_4OH at 90 $\pm$ 10°C for 5 minutes.
  - Soak web in freshly prepared 5:1:1 H_2O: H_2O_2: HCl at 90 $\pm$ 10°C for 5 minutes.
- Diffusion Conditions:
  - Source - BBr_3
  - Material used (4-inch diameter tube) - 2.25 ℓ/min Ar, 20 cc/min O_2, 2 mg/min BBr_3. Note: 2 mg/min BBr_3 can be obtained by bubbling 7.4 cc/min Ar through liquid BBr_3 at 0°C.
  - Temperature - 950°C
  - Predep time - 37 min
  - Strip diffusion glass and SILOX layer with 3:1 H_2O: HF for 30 seconds.

Process Control:

Sheet resistance of 60 $\pm$ 10 Ω/□.

3. Phosphorus Diffusion

In this step the front n^+p junction is formed.

Process Specifications

- Apply a SILOX diffusion mask of thickness 5000 $\pm$ 500 Å at 420°C to the back side of the web. (Back side is side with ID number).

- Clean web with:
  - Dip in 10:1 H_2O:HF for 15 seconds.
  - Soak web in freshly prepared 5:1:1 H_2O:H_2O_2: NH_4OH at 90 $\pm$ 10°C for 5 minutes.
  - Soak web in freshly prepared 5:1:1 H_2O:H_2O_2: HCl at 90 $\pm$ 10°C for 5 minutes.
- Diffusion Conditions:
  - Source $POCl_3$
  - Material used (4-inch diameter tube) - 1.2 ℓ/min N_2, 20 cc/min O_2, 5 mg/min $POCl_3$. Note: 5 mg/min $POCl_3$ can be obtained by bubbling 61 cc/min N_2 through liquid $POCl_3$ at 0°.
  - Temperature - 850°C
  - Predep time - 30 minutes
- Strip diffusion glass and SILOX layer with 3:1 H_2O:HF for 30 seconds.

Process Control:

Sheet resistance of 60 $\pm$ 10 Ω/□.

4. Deposition of Anti-Reflection Coating

The process defined requires an anti-reflection (AR) coating to be applied to the web before metallization. This AR coating acts as a mask in the subsequent plating operating.

Process Specification:

AR Solution: The solution is prepared by controlled hydrolysis and polymerization of titanium alkoxides having a general formula of $Ti(OR)_4$, where R is an alkyl. An example of a titanium alkoxide which has been used successfully is titanium tetra-ethoxide, $Ti(OC_2H_5)_4$. The hydrolysis is performed in an alcohol medium, such as ethyl alcohol, $C_2H_5(OH)$. In order to adjust the index of refraction of the AR coating for an optimum match to silicon, a silicon alkoxide solution is prepared and mixed with the titanium alkoxide solution. An example of an appropriate silicon alkoxide is silicon

tetra-ethoxide, $Si(OC_2H_5)_4$. Details related to the preparation and curing of the AR coating are considered proprietary, and an application for a patent to cover these areas has been filed.

Application: The AR solution is applied by withdrawing the web from the AR solution at a controlled rate of 30 $\pm$ 3 cm/min.

Drying: The coated silicon web strips are heated in air to 400°C and are held at 400°C for 5 minutes. The composition of the cured AR coating is 88% TiO_2 and 12% SiO_2. Additional information related to the performance and characterization of the AR coating can be found in the paper "Antireflective Coatings Applied from Metal-Organic Derived Liquid Precursors," Yoldas, B. E. and T. W. O'Keeffe, Applied Optics, 18, 1979, p. 3133.

Process Control:

- Color of anti-reflection coating on n^+ side of web should be dark blue-black.
- Film thickness 750 Å $\pm$ 50 Å and Index of Refraction 2.00 $\pm$ 0.05, as measured by an ellipsometer.

5. Deposition of Photoresist

A photoresist layer must be applied to the web (over the AR coating) so that photolithographic techniques may be used to define the conductive grid pattern.

Process Specification:

- Prepare a 50/50 solution of AZ1350J photoresist and AZ thinner (produced by Shipley Co.).
- Immerse web, lengthwise in above solution and withdraw at 25 cm/min. $\pm$ 5 cm/min. to obtain a 1 to 2 μm coating of photoresist.
- Bake web at 90°C $\pm$ 3°C for 15 min. $\pm$ 3 min.

Process Control:

Photoresist coating should be free of obvious pinholes.

6. Exposure and Development of Grid Pattern

Standard photolithographic techniques are used to define a grid pattern through the PR and AR and thus form a metallization pattern.

Process Specification:

- Use negative mask fabricated on a plastic base; mask to fit between dendrites and lay on web.
- Expose photoresist with 55 millijoule/cm^2 for approximately 10 secs.
- Develop grid in photoresist using 80/20 AZ developer and DI water, at 23°C $\pm$ 4°C for 60 sec. with mild agitation (AZ Developer produced by Shipley Co.).
- Rinse in DI H_2O; 8 megohm minimum.
- Bake at 120°C $\pm$ 3°C for 15 minutes $\pm$ 3 minutes.
- Develop grid in anti-reflection coating using etch composed of 150 parts DI H_2O, 60 parts HCl, and 30 parts NH_4F with a 3-second immersion.
- Wash in DI H_2O; dry with forced, filtered air.

Process Control:

Width of grid lines to be 25 µm $\begin{cases} +\ 5\ \mu m \\ -\ 0\ \mu m \end{cases}$

7. Metallization

Thin layers of metal are evaporated over the entire surface of the cell. These metals serve as plating base for the electroplated conductive layer. The Ti serves as a barrier metal to prevent diffusion of conductive metals into the silicon.

Process Specification:

- Place web in evaporation system and pump system to 1 x 10^{-6} Torr.
- Evaporate 500 Å $\pm$ 50 Å of Ti, at 15 $\pm$ 3 Å/sec.

- Evaporate 300 Å ± 50 Å of Pd, at 10 ± 3 Å/sec.
- Evaporate 300 Å ± 50 Å of Ag, at 10 ± 3 Å/sec.
- Evaporation takes place over entire front surface of web.

Process Control:

Metal layer thickness can be checked using glass control slide and "Talystep" apparatus.

8. Rejection of Excess Evaporated Metal

Since the thin metal has been evaporated over the entire cell, those parts of the metal layers overlaying the photoresist are rejected by dissolving the photoresist.

Process Specification:

- Immerse web in acetone for 5 minutes with mild agitation.
- If any metal remains on silicon after this time, swab with cotton and acetone.
- Rinse in clean acetone bath.
- Rinse in methanol bath.
- Dry in forced clean air.

Process Control:

No metal on cells other than in grid areas.

9. Preparation of Conductive Grid by Electroplating

The thin metal layers in the grid pattern cannot carry the current produced in the solar cell without excessive series resistance. Therefore, a thick conductive layer is electroplated on top of these layers.

Process Specification:

- Web in holder immersed in plating solution (see below) and plated at 10 mA/cm^2 for 15 minutes. (Area is area to be plated, i.e., back of web plus grid on front.)

- Web washed in DI H_2O for 5 minutes and dried in forced, clean air.

Process Control:

Plated Cu to be 8 μm ± 2 μm.

Cu Plating Solution:

Volume as required DI H_2O, 187 g/ℓ $CuSO_4 \cdot 5H_2O$, 21 mℓ/ℓ H_2SO_4 (concentrated)

Anode - Phosphorized copper (1.5% - 4.5% phosphorus, oxygen free) from Udylite Division of Oxy Metal Industries.

Use at 23°C ± 3°C with vigorous agitation.

10. Laser Scribing

Up to this point in the process, the cells have been fabricated on long lengths of web with the dendrites in place. The individual cells are separated from the web by laser scribing from the back and breaking out the cell.

Process Specification:

- Align cell on holder* with back of cell facing laser beam.
- Scribe cell periphery with Nd-Yag laser. (Nominal power 3-5 watts repetition rate - 1000/sec.)

Process Controls

Cell area = A_o ± 0.5%. (Nominal cell size is (2 x 10) cm.)

No cracks or chips on cell.

Laser penetration from back 60 μm $\{^{+\ 0}_{-\ 10}$ μm.

*A holder has been developed for this process which permits the cell to be aligned with the laser beam by observing the front of the cell in a 45° mirror. A patent application describing this holder has been filed.

11. Cell Testing

All cells are tested. After testing, they are categorized as to final parameters.

Process Specification:

- Parameters to be measured:

  V_{oc}

  I_{sc}

  V at I = 0.9 I_{sc}

  V at I = 0.8 I_{sc}

  V at I = 0.7 I_{sc}

- From these parameters determine: (1) open-circuit voltage, (2) short-circuit current, (3) fill factor, (4) efficiency, (5) I and V at peak power.

Process Control:

Cells meet specifications or can be properly classified.

12. Cell Interconnection Into Strings

In this step, cells are interconnected using ultrasonic bonding.

Process Specification:

- Prepare aluminum interconnect preforms (35 μm thick)
- To each contact pad on the front of the cell bond a tab of the interconnect.
- Interconnect required number of cells into a series string by bonding the aluminum interconnect attached to the front of one cell to the back of the next cell in the string.
- Bond copper foil to the aluminum interconnects at the top and bottom of the string.

Process Control:

Cells are not to be cracked and bonds are to be adherent.

13. Encapsulation

The cell strings are sealed into a protective package and electrical connectors are attached.

Process Specification:

- Clean and prime the cover glass.
- Layup the package as follows:
  - Glass plate
  - Ethylene Vinyl Acetate
  - Solar Cell Strings
  - Craneglass
  - Ethylene Vinyl Acetate
  - Korad
  - Teflon
  - Aluminum Sheet
- Place layup in vacuum bag lamination apparatus and pump out both chambers of the apparatus.
- Heat to 110°C in about 20 minutes, then vent top chamber to atmosphere, thereby causing a uniform pressure to be applied to the layup.
- Continue to heat to 150°C takes an additional 11 minutes, then stop heating.
- Cool to room temperature in about 30 minutes.

- Remove Teflon and aluminum sheets from the layup.
- Epoxy electrical connectors to the back of the module after soldering copper tabs at the ends of the strings to the connector contacts.

Process Control:

Encapsulated module should be free of air bubbles and encapsulation should not crack cells.